DETERMINATION OF RESOLUTION, REPEATABILITY, AND DETECTION CAPABILITY IMPROVEMENTS OF AUTOMATIC OPTICAL INSPECTION IN MICRO-ELECTRO-MECHANICAL SYSTEMS MANUFACTURING

Lappeenranta-Lahti University of Technology LUT

Master's Program in Computational Engineering, Master's Thesis

2022

Tiina Nurmi

Examiners: Professor Bernardo Barbiellini
Ph.D. Sami Kujala

ABSTRACT

Lappeenranta-Lahti University of Technology LUT
School of Engineering Science
Computational Engineering

Tiina Nurmi

Determination of Resolution, Repeatability, and Detection Capability Improvements of Automatic Optical Inspection in Micro-Electro-Mechanical Systems Manufacturing

Master's thesis
2022
61 pages, 26 figures, 10 tables, 3 appendices
Examiners: Professor Bernardo Barbiellini and Ph.D. Sami Kujala

Keywords: automatic optical inspection, MEMS, image processing

Automatic optical inspection (AOI) is a quality monitoring system used in many industries. In semiconductor industry, it is used to detect anomalies, inter alia, defects in wafers and micro-electro-mechanical systems (MEMS). AOI is an automated optical microscope whose resolution is determined by Rayleigh's equation and the design of the camera. The objectives of the thesis were to determine the capability of the AOI equipment at Murata Electronics Oy in terms of resolution and repeatability, and investigate potential capability improvement suggestions. The experiments were delimited to structure wafers and surface inspection. Overall, the smallest resolution can be achieved by using short wavelength, big magnification, and sensitive inspection characteristics. In addition, the topography of the defects and the materials on the surface of the wafer must be taken into account so that the contrast of the defect images and the signal-to-noise ratio (SNR) are improved. The smallest resolution of the AOI equipment was obtained with 10X magnification and sensitive inspection characteristics. The capability of the device can be improved by dividing the inspection into tests in which the critical areas of the element are inspected with 10X magnification, short wavelength, and sensitive inspection characteristics. For other element areas, less sensitive inspection characteristics can be used. Other inspection techniques, such as an automated scanning electron microscope (SEM), must be considered to exceed the resolution limit of the visible light.

TIIVISTELMÄ

Lappeenrannan-Lahden teknillinen yliopisto LUT
School of Engineering Science
Laskennallinen tekniikka

Tiina Nurmi

Automaattisen optisen tarkastuksen resoluution, toistettavuuden sekä tarkastuskyvykkyysparannuksien määrittäminen mikroelektromekaanisten järjestelmien tuotannossa

Diplomityö
2022
61 sivua, 26 kuvaa, 10 taulukkoa, 3 liitettä
Tarkastajat: Professori Bernardo Barbiellini ja TkT Sami Kujala

Hakusanat: automaattinen optinen tarkastus, MEMS, kuvankäsittely

Automaattinen optinen tarkastus (AOI) on menetelmä, jota käytetään laadun monitoroinnissa useilla eri teollisuuden alueilla. Puolijohdeteollisuudessa AOI on toiminut kiekkojen ja mikroelektromekaanisten järjestelmien (MEMS) poikkeavuuksien eli defektien detektoinnissa. AOI on automaattinen valomikroskooppi, jonka resoluution määrittää Rayleighin yhtälö ja kameran ominaisuudet. Diplomityön tavoitteena oli selvittää Murata Electronics Oy:n AOI-laitteen kyvykkyys resoluution ja toistettavuuden suhteen, sekä tutkia mahdollisuuksia parantaa laitteen kyvykkyyttä. Tutkimus rajattiin koskemaan rakennekiekkoja ja pinnan tarkastusta. Yleisesti, pienin resoluutio saadaan käyttämällä lyhyttä aallonpituutta, isoa suurennosta, ja herkkiä tarkastusparametreja. Näiden lisäksi täytyy huomioida defektien topografia sekä kiekon pinnan materiaalit, jotta voidaan parantaa defektikuvien kontrastia ja signaali-kohinasuhdetta (SNR). AOI-laitteen pienin resoluutio saavutettiin 10X suurennoksella ja herkillä tarkastusparametreilla. Laitteen kyvykkyyttä voidaan parantaa jakamalla tarkastus testeihin, joissa elementin defekteille kriittiset alueet tarkastetaan 10X suurennoksella, lyhyellä aallonpituudella, ja herkillä tarkastusparametreilla. Muille alueille voidaan käyttää vähemmän herkkiä tarkastusparametreja. Näkyvän valon resoluutiorajan ylittämiseksi täytyy harkita muita tarkastustekniikoita, kuten automatisoitua pyyhkäisyelektronimikroskooppia (SEM).

ACKNOWLEDGEMENTS

I would like to thank Murata Electronics Oy for giving me the opportunity to develop my skills and expertise in the area of MEMS element manufacturing. A great thank you to the WAVI team for giving me interesting challenges to work with, not forgetting the topic of the thesis. It has been a pleasure to work with you.

I would like to thank my supervisors, Sami Kujala and Bernardo Barbiellini. Thank you for supporting me throughout the thesis. Your knowledge and feedback has been valuable.

A great thank you to my friends and family for standing by my side. A special thank you for Rosa, Henriikka, and Antti for making the years at the university unforgettable. I want to thank my lovely friend Riikka for all these years since kindergarten. You have always shed a light to my life, and especially during the thesis, it has been worth of gold.

But in the end, through a couple of twists and turns, here I am as a Master of Science! These past years have been the best time of my life and I wouldn’t change a second. So, a big thank you to the calculator that decided not to work in the 2017 veterinary entrance exam.

Helsinki, June 1, 2022

Tiina Nurmi

LIST OF ABBREVIATIONS AND SYMBOLS

ABBREVIATIONS

AOI	Automatic Optical Inspection
BF	Brightfield
CCD	Charge Coupled Devices
CMOS	Complementary Metal Oxide Semiconductor
CNN	Convolutional Neural Network
F	Focal Point
FL	Focal Length
DF	Darkfield
DLP	Digital Light Processing
DOI	Defect of Interest
DRIE	Deep Reactive Ion Etching
FBAR	Film Bulk Acoustic Resonator
FOV	Field of View
GAGE R&R	GAGE Repeatability & Reproducibility
LED	Light Emitting Diode
MEMS	Micro-Electro-Mechanical Systems
NA	Numerical Aperture
PCB	Printed Circuit Boards
RF	Radio Frequency
SEM	Scanning Electron Microscope
SNR	Signal-to-Noise Ratio
SOM	Self-Organizing Map
SSIM	Structural Similarity Index
SVM	Support Vector Machine
SZ	Image Sensor Area
WD	Working Distance
Z	Depth of Field

SYMBOLS

α Half-angle of objective's collection cone

λ Wavelength of light

a Distance between object and lens

b Distance between image and object

d Distance between two adjacent particles

f Focal Length

I Intensity

n Index of refraction

CONTENTS

1 INTRODUCTION 8
- 1.1 Background . . . 8
- 1.2 Objectives and delimitations . . . 9
- 1.3 Structure of the thesis . . . 9

2 HISTORY AND INTRODUCTION OF MEMS 11

3 ARCHITECTURE OF AUTOMATIC OPTICAL INSPECTION 13

4 DEFECT DETERMINATION 23
- 4.1 Definition of a defect . . . 23
- 4.2 Detection . . . 24
- 4.3 Image processing . . . 27

5 DETECTION CAPABILITY IMPROVEMENTS 32

6 EXPERIMENTS 34
- 6.1 Experiment wafers . . . 34
- 6.2 Inspection recipes . . . 35
- 6.3 Data . . . 36
- 6.4 Description of experiments . . . 37
- 6.5 Repeatability and resolution analysis . . . 38
- 6.6 Accuracy analysis . . . 49
- 6.7 Difference image analysis . . . 51

7 DISCUSSION 55
- 7.1 Current study . . . 55
- 7.2 Future work . . . 57

8 CONCLUSION 58

REFERENCES 59

APPENDICES
- Appendix 1: Wafer map figures
- Appendix 2: Stacked die figures
- Appendix 3: Median relative standard deviations for the defect attributes

1 INTRODUCTION

1.1 Background

Automatic optical inspection (AOI) is a system which has various applications such as inspection, measurement, classification, product sorting, object positioning, and process monitoring. AOI has had a rapid development recent years along with industries such as semiconductors and printed circuit boards (PCB). With AOI, it is possible to measure the quality and properties of the inspected object. It can output information about the dimension, structure, and position of the inspected object and its defects. In the past, manual inspection methods were used to investigate the quality of various products. Manual inspection has several quality issues such as inefficiency and false or missed detection due to discrimination ability. There are also challenges with the human eye. The resolution of the eye is limited and can be easily fatigued. Overall, manual inspection is not capable for complex and small structures, so AOI had to be developed. AOI has mostly replaced human manual inspection as it has overcome the challenges regarding manual inspection such as repeatability, resolution, discrimination ability, yield, and performance. [1–3]

In semiconductor industry, AOI is used in quality monitoring of, inter alia, bare wafers and wafers patterned with micro-electro-mechanical systems (MEMS). It can be implemented in tool monitoring, process monitoring, or at the end of the manufacturing process to detect anomalies in the equipment's performance, process, or at the end product [1]. AOI is capable to detect defects and defect patterns. With the help of AOI, element failure root causes can be identified [4]. The detection of a defect is a process where the first problem is the actual detection of the defect [5]. To overcome this problem, various light sources and illumination techniques are used. The second problem is how to separate real defects from nuisance defects [5].

The future demands in the semiconductor industry are related to cost reduction, yield improvement, and miniaturisation of semiconductor device structure [6]. New technology nodes include smaller structures one another. Previously irrelevant defects become killer defects which can cause critical damage to semiconductor devices [5]. Therefore, the capability of the current AOI equipment at Murata Electronics Oy must be determined in terms of resolution and repeatability.

The capability of the AOI equipment is determined with patterned wafers containing programmed defects. The repeatability, resolution, and accuracy are determined by inspect-

ing the experiment wafers 10 times under the same conditions. The defect coordinates from repeated inspections provided by the AOI equipment are matched together. This reveals which defects are detected repeatedly. Repeatability measures how well the outcome of the inspection can be repeated under the same conditions. The inspection is not reliable if the repeatability is poor. Therefore, resolution is determined as the smallest defect bounding box area which is detected with a 90 % probability. That is, the area which is detected repeatedly in 9 out of 10 inspections. The accuracy is determined as the uncertainty of the defect attributes such as defect coordinates and area.

1.2 Objectives and delimitations

The objective of the thesis was to determine the capability of AOI equipment at Murata Electronics Oy in terms of repeatability and resolution. Also, future capability improvements and trends of AOI technology were investigated. To support the objectives of the thesis, a comprehensive literature review of AOI was conducted. The objectives of the thesis could be divided into the following research questions:

1. What is the current resolution of the AOI equipment at Murata Electronic Oy?
2. What is the current repeatability of the AOI equipment at Murata Electronics Oy?
3. How the capability of the AOI can be improved?

The thesis was delimited to surface inspection because the AOI equipment is used for surface inspection only. In addition, the experiments were conducted on structure wafers which contain the detailed and fragile sensor structures.

1.3 Structure of the thesis

The thesis begins with a short introduction to MEMS and its history in Chapter 2. Then, Chapter 3 presents a comprehensive literature review of the topics related to the architecture of AOI equipment. In addition, the definition of resolution is defined, and the properties of AOI equipment affecting to the resolution are discussed. The process of defect determination is explained in Chapter 4. First, the definition of a defect is explained with a few examples. It is followed by sections discussing about detection and

image processing. The state-of-the-art and future trends related to detection capability improvements of AOI technology are reviewed in Chapter 5.

The experimental part is presented in Chapter 6. The wafer material and inspection recipes are first introduced. Then, the experiments conducted for the wafers are listed. Lastly, the results are presented. First, the results for repeatability and resolution are discussed. Then, the accuracy of the detect attributes are presented. Lastly, the results of difference image analysis are reported.

Finally, further analysis of the results and detection capability improvements are discussed in Chapter 7. The conclusions are given in Chapter 8.

2 HISTORY AND INTRODUCTION OF MEMS

The first steps in the technology of MEMS can be dated to 1954 at Bell Telephone Laboratories, where a paper of stress sensitive effects in silicon and germanium, piezoresistance, was published. In the early 1960's, first silicon diaphagram pressure sensors and strain gauges were introduced. However, the actual first electro-mechanical device in the scale of a micron was fabricated in 1967 with Resonant Gate Transistor. It did not take long until the first commercial MEMS products were released to commercial markets. In the 1970's and early 1980's pressure sensors and HP ink jet nozzles were introduced. Later in the 1990's, accelerometers manufactured by Analog Devices Inc. were introduced in automotive airbags and digital light processing TV's. Another great success was film bulk acoustic resonator radio frequency filter invention from Avago. The development of MEMS products took a long time and required new techniques in process, structure, packaging, and test methods. The milestones of MEMS products and technology developments are arranged in the Figure 1. It shows how the number of new products and technologies is growing from left to right. [7, 8]

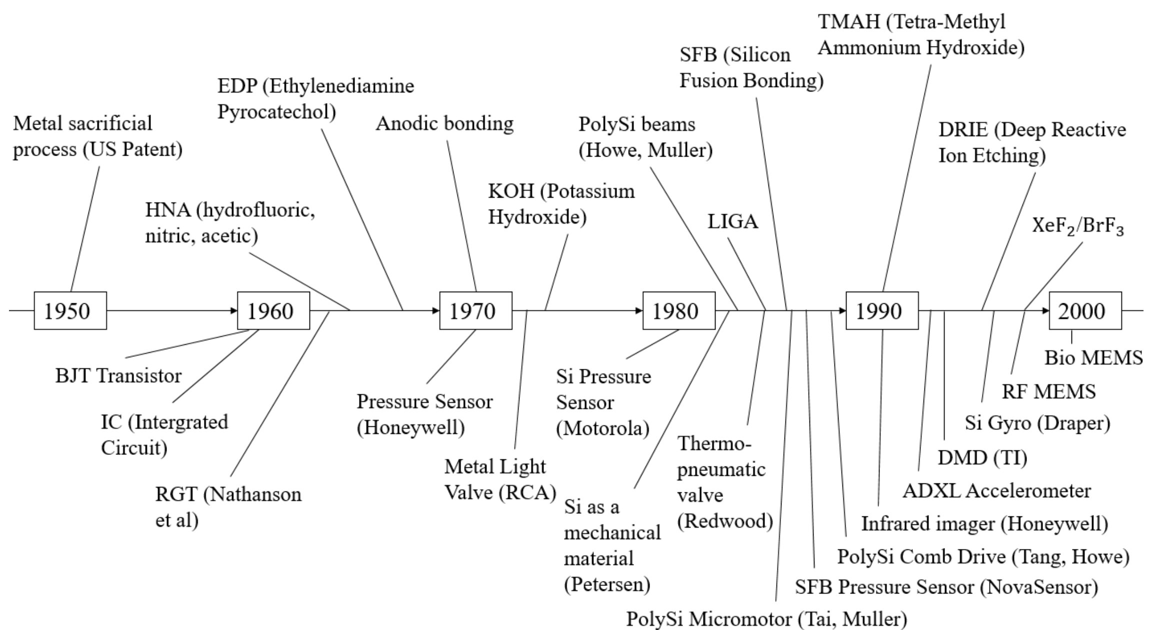

Figure 1. The most significant milestones in MEMS development. At the top of the figure are MEMS technology related milestones. At the bottom are MEMS product related milestones. [7]

The operating principle behind the first pressure sensor was based on the piezo-resistive effect which was used to sense pressure-induced strain on membranes. The structure of the sensor was produced with backside etching so that the membrane material with

piezo-resistors was leaved on the surface. When traditional semiconductor processes of patterning, deposition, and etching were introduced to MEMS manufacturing, the popularity of MEMS increased. The first structures made with these techniques were gears and motors having only low volume applications. Process development was required so that more complex MEMS structures could be processed. Development of deep reactive ion etching (DRIE) and bonding methods resulted in high performance inertial sensors which could be applied in automotive airbags. With silicon bonding or fusion bonding, bulk single crystal silicon layer could be laminated as a thicker alternative to the polysilicon structural layer, and wafers could be encapsulated. This enabled cost effective vacuum packaging. Complementary Metal Oxide Semiconductor (CMOS) wafer bonding enabled mechanical micro-package and interconnections between mechanical device and circuit. [7]

MEMS sensors are capable to measure the changes in the environment in terms of mechanical, magnetic, chemical, optical, acoustic, thermal, and electromagnetic information. The physics behind MEMS sensors are based on different methods such as piezoresistive, piezoelectric, capacitive, electromagnetic, and thermal electrical methods. Accelerometers have moving masses which are under stress when applied into external acceleration. The stress results in differential signal, differential frequency, voltage output, resistance variance, or capacitance variation. Gyroscopes measure the angular variance or angular rate with Coriolis force. Acoustic sensors have capacitive sensing mechanism. They are used in consumer electronics such as smart phones and speakers. Gas sensors are applied in gas quality measurements. They measure the band gap energy resulting in resistance change. [7, 9]

Advantages of MEMS include small size, high signal-to-noise ratio (SNR), low hysteresis, durability of extreme environments, and high fabrication repeatability. These advantages have enabled different applications for MEMS such as automation, aeronautics, consumer electronics, and medical equipment. However, new challenges have occurred as the demands have tightened. MEMS sensors must be more intelligent and less power consuming. They must also have mutual interaction capability in human-machine interface applications. [9]

3 ARCHITECTURE OF AUTOMATIC OPTICAL INSPECTION

The architecture of an AOI equipment is built of multiple components and is usually designed and delivered to fit the needs of a customer [10]. The architecture shown in the Figure 2 can be broken down to two main components - hardware and software. The hardware is basically an automated light microscope which consists of the motion control system, lenses, light illumination modules, image acquisition modules, industrial computers, and additional processing units [1, 10].

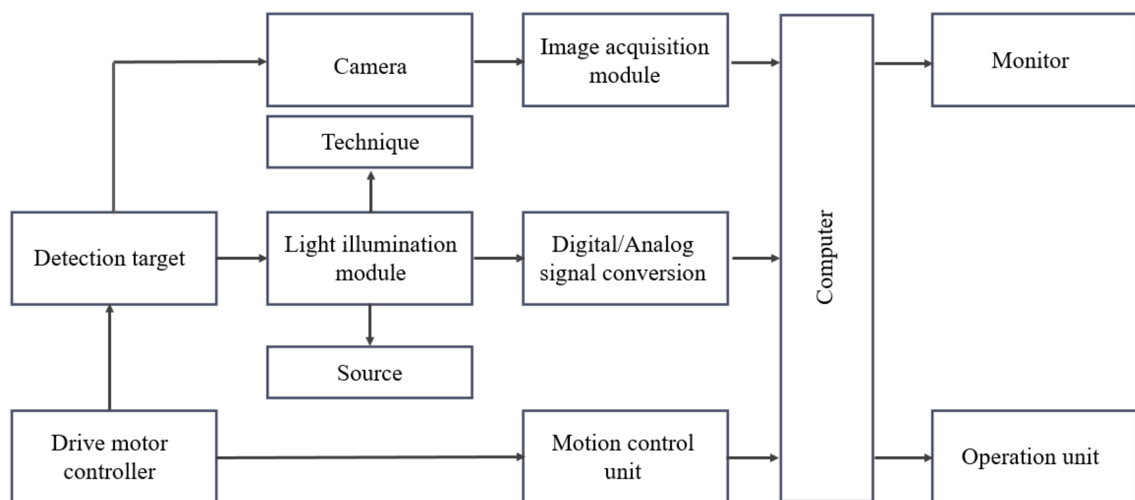

Figure 2. Logical structure of AOI.

Optical microscope is composed of two lens types - objective lenses and condenser lenses. Objective lenses are used to gather the diffracted light from the object to form a magnified image. Condenser lenses focus the light from the illuminator onto a small area on the object. The lens can be positive or negative - positive lenses magnify the image and negative lenses demagnify the image. Positive lens combines parallel incident rays and forms a real image, negative lens scatters the incident rays and does not form a real image. A simple lens has two refracting surfaces and two planes - principal and focal. The principal plane is within the lens in which the incident and emergent rays intersect. The focal plane is in the focused image in which rays intersect to form the image. The focal length f is the distance from the principal plane to the focal point F. The distance a of the object is the distance between object and the principal plane, and respectively, the image distance from the principal plane to the formed image is denoted as b. [11] The

relationship between the focal length f and the distances a and b of the object and image can be described with an equation, often denoted as the thin lens equation

$$\frac{1}{f} = \frac{1}{a} + \frac{1}{b}. \tag{1}$$

The geometrical parameters presented in the lens equation above are visually shown in Figure 3.

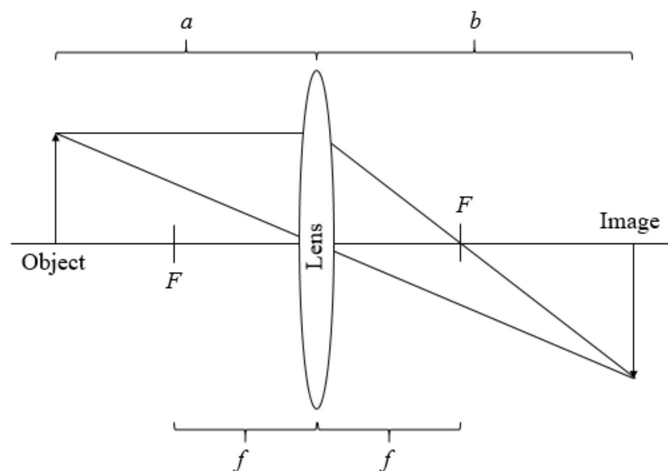

Figure 3. Geometric parameters of a simple thin lens describing the image formation in light microscope. Focal length f is the length from the principal plane of the lens to the focal point F. The value is the same for both front and rear focal lengths. Parameter a denotes the distance from the object to the principal plane of the lens whereas b describes the distance from the image to the principal plane.

The distance of the inspected object and the focal point of the lens determine whether the image is magnified or demagnified. It also defines whether the image is real or virtual. In principal, if the distance a of the inspected object is below the focal length f, the formed image is virtual and magnified. If the object distance a is equal to the focal length f, the distance of the image is infinite. Therefore, no image can be formed. These relationships between the object and the image are shown in Figure 4. [11]

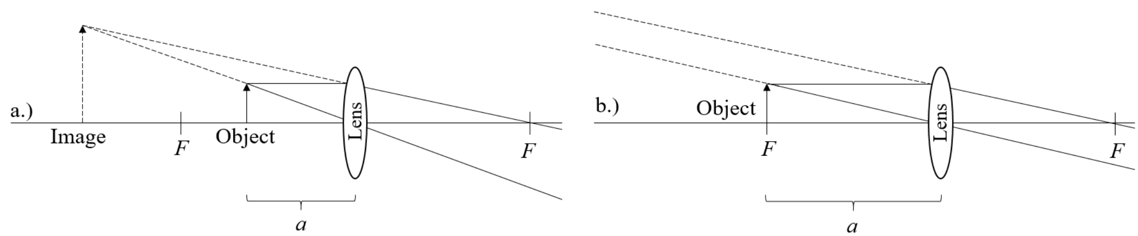

Figure 4. The relationships between the inspected object and formed image when $a \leq f$. In figure a.) a virtual and magnified image of the inspected object is formed when $a < f$. In figure b.) no image is formed because the distance of the image is infinite when $a = f$.

Figure 5 visualizes the relationships between the object and the image when the distance a of the inspected object is greater than the focal length f. A real and magnified image is formed when the distance of the inspected object is greater than the focal length but smaller than the doubled focal length. If the distance of the inspected object is equal to the doubled focal length, the magnification remains the same and a real image is formed. Demagnification occurs when the distance of the inspected object is greater than the doubled focal length. [11]

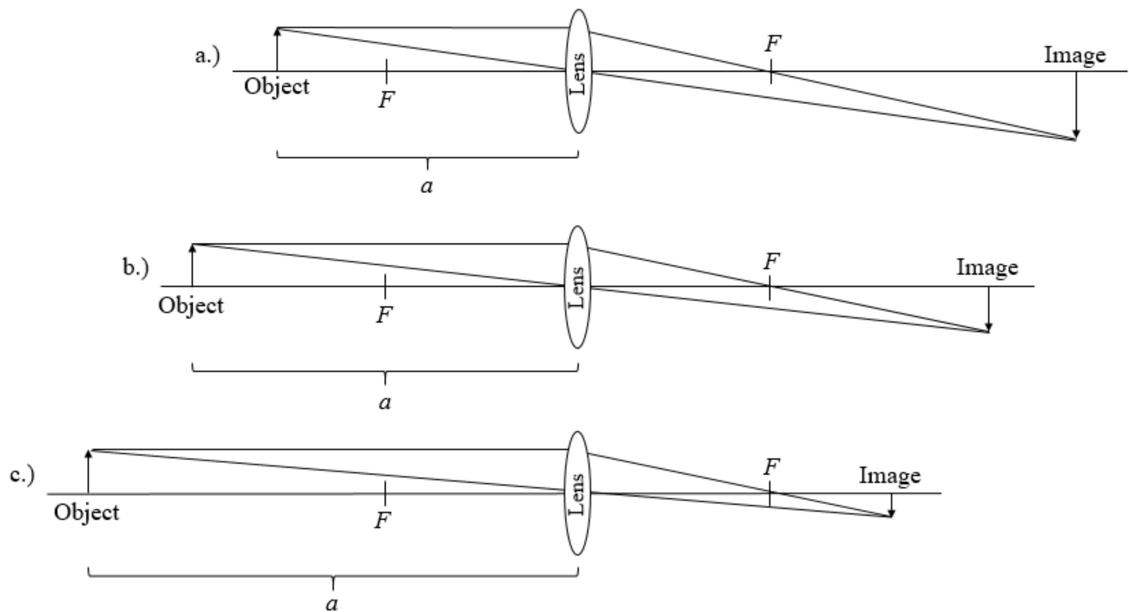

Figure 5. The relationships between the inspected object and formed image when $a > f$. In figure a.) the condition is $f < a < 2f$. The formed image is real and magnified. In figure b.) the formed image is real. The magnification remains the same because the condition is $a = 2f$. In figure c.) the condition is $a > 2f$. Therefore the image formed is real and demagnified.

Magnification is the combination of resolution and detector pixel size. The resolution of

an optical microscope is not only dependent of the magnification. Magnification can be considered as the relative enlargement of the image over the object. It is limited to the resolution of the instrument itself. Therefore, using the highest magnification available is not necessarily the most effective solution to achieve small resolution. [12]

Numerical aperture determines the acceptance angle for light. The acceptance angle in turn determine the gathering power of light, the resolving power of the microscope, and the depth of field of the objective. Mathematically the numerical aperture can be expressed as

$$\text{NA} = n \times \sin \alpha, \tag{2}$$

where n is the index of refraction of the immersion medium and α is the half-angle of the objective's collection cone [12]. The higher the numerical aperture, the more light will be collected, and the better the resolution [11]. The parameters affecting to the numerical aperture are visually shown in Figure 6.

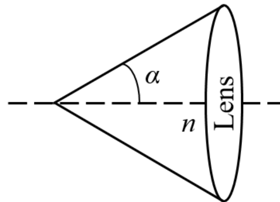

Figure 6. The parameters affecting to the numerical aperture NA. The greater the half-angle α of the objective's collection cone and the index of refraction n of the immersion medium, the larger the numerical aperture.

Resolution is the smallest distance in which two objects can be apart and treated as two separate objects [12]. In an ideal optical system, the resolution is only limited by the diffraction principles of light. Due to which, the resolution can be simply determined with Rayleigh's equation

$$d = 1.22 \left(\frac{\lambda}{2\text{NA}} \right), \tag{3}$$

where d is the distance between two adjacent particles, λ is the wavelength used, and NA

is the numerical aperture of the objective [13]. If the inspected sample is small in size, the value for numerical aperture should be high. This is because small samples typically transmit more higher diffracted orders to the objective. Respectively, shorter wavelengths have better resolution [13]. According to the Rayleigh's criterion, two adjacent points can be defined resolved when the central diffraction spot of one point coincides with the first diffraction minimum of the other point in the focal plane as presented in the Figure 7. The resolution limit can be applied to two points of light under dark field illumination or under incoherent illumination [11].

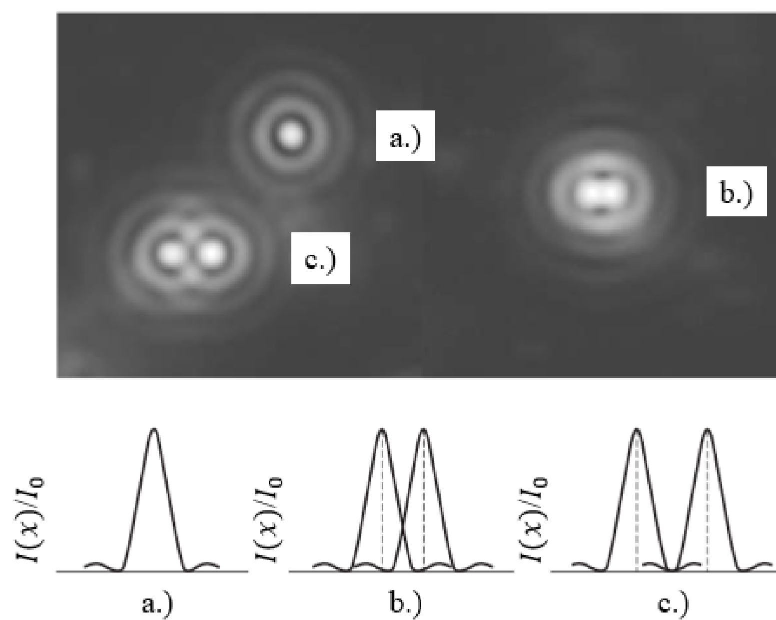

Figure 7. Rayleigh's criterion presented visually with $I(x)/I_0$ curves and diffraction patterns. A single diffraction pattern is shown in figures marked with a.). The Airy disk and 1st and 2nd order diffraction rings are visible. In figures marked with b.) the disk maximums overlap with the first minimums. So, the points are just resolved. If the disk maximums overlap with the second minimums, the points are clearly resolved as shown in figures c.). The figure was retrieved from [11] and modified.

Light illumination modules determine what properties of the wafer surface are highlighted and attenuated. This is because the combination of illumination properties such as the wavelength, angle, luminance, and uniformity affect in the overall quality of the defect imaging [1]. Therefore, it might be beneficial to have multiple light illumination modules with different light sources and illumination structures so that all defect types and sizes could be detected. The suitability of the light source wavelength is based on the absorption and reflection properties of the inspected object and the background [1]. In addition, it is necessary to consider that the light source does not damage the inspected object. The

penetration of the inspection light is better with longer wavelengths, and the diffusion is better with shorter wavelength. Typical examples of light sources, their properties, and applications are shown in Table 1. As an example, infrared light is used when the inspection object is below the surface, and blue light is used for surface inspection. The most common light sources used in AOI are light emitting diodes (LED), fluorescent, quartz-halogen, ultraviolet, and infrared. [1, 10]

Table 1. Light sources, their wavelengths, and common applications in wafer inspection. [14]

Light source	**Wavelength**	**Applications**
White light	Multi-wavelength	Color images, wide range of applications
Blue light	430-480 nm	Suitable for products with silver colored backgrounds
Green light	510-530 nm	Suitable for products with red or silver colored backgrounds
Red light	600-720 nm	Can pass through dark objects which absorb most wavelengths, can improve image contrast, line detection and light transmission film thickness detection
Infrared light	780-1400 nm	Capable to detect defects sandwiched between silicon wafers
Ultraviolet light	190-400 nm	Reticle inspection, unpatterned wafer surface inspection
X-ray light	0.01-10 nm	Better resolution

The structure of illumination module can be divided into forward and back illumination as shown in Figure 8. Forward illumination uses reflected light whereas back illumination uses transmitted light. Forward illumination is capable to detect surface defects, scratches, and the surface texture features. It is the most widely used illumination method. Back illumination can observe the interior of transparent objects and highlight the shadow of opaque objects. It is used in shape and dimension detection. Forward illumination can be modified into coaxial or scattering forward illumination. In coaxial forward illumination, the light is passed trough a half-mirror so that the light coaxial with the lens is formed. Coaxial light is uniform, has high intensity, and avoids the reflection of the object. It is basically a more accurate and reproducible version of forward illumination. Scattering forward illumination consist of a dome structure. It is used in solder joint and chip pin detection. [14]

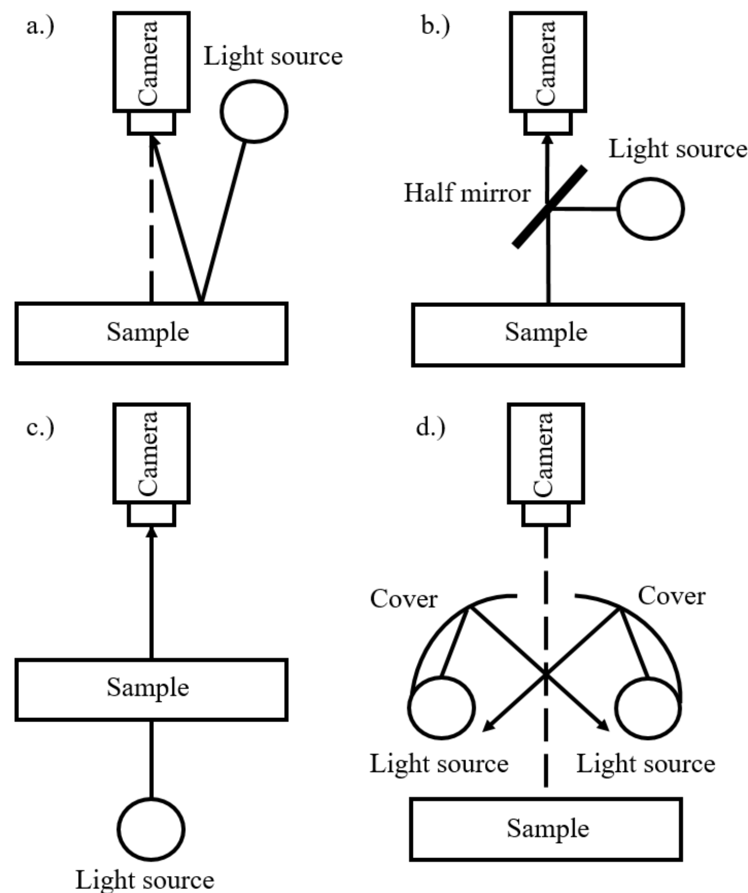

Figure 8. Sketch of the structures of different illumination modules: a.) Sketch of forward illumination in which the light source and camera are on the same side.; b.) Coaxial illumination is a modification of forward illumination. A half mirror is added so that reflections are avoided, and the uniformity and intensity of light is increased.; c.) Back illumination in which the light source is behind the object.; d.) Scattering forward illumination is another modification of forward illumination. The covers create a dome structure.

Illumination angle is the angle between the surface of the illuminated object and the illuminator itself. The most common illumination technique is brightfield, but there are also on-axis, darkfield, and back light illumination. The incidence angle in brightfield is almost perpendicular to the inspected surface. As a result, most of the reflected light is captured by the sensor. So, the surface of the inspected object is bright and the defect appears in gray levels. Darkfield is the opposite of brightfield as the angle of the incident light in darkfield is relatively large. Thereby, the light collected by the sensor is mostly scattered light. So, the surface of the inspected object is dark and the defects are bright. The difference in brightfield and darkfield illuminations are shown in Figure 9. Darkfield illumination is capable to detect the edge and height of the surface. It has a great performance on the surface concavity and convexity. [1, 14, 15]

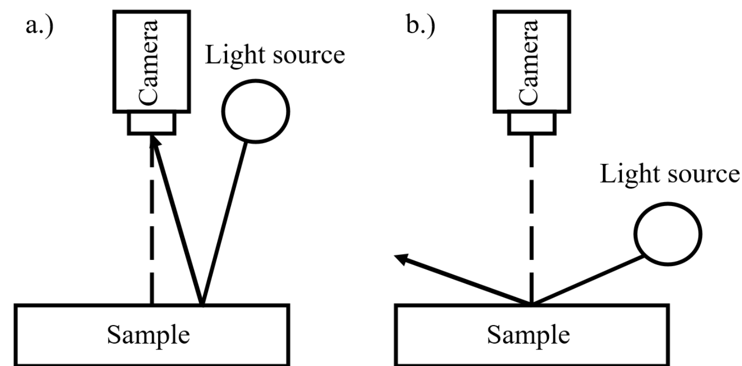

Figure 9. Sketch of brightfield and darkfield illumination techniques: a.) Sketch of a brightfield illumination in which the angle of the incident light is almost perpendicular to the surface of the inspected sample.; b.) Sketch of darkfield illumination in which the angle of incident light is relatively large.

The image acquisition system retrieves the analog image signal of the defect, converts the analog signal into digital signal, and transmits the digital images into a computer. There are three main image acquisition methods used to capture the defects on the wafer surface. The first method is flying spot scanning where a light spot is focused on the detected surface, and the surface is scanned with high speed on X and Y directions. The scattered light is collected with photodiodes or photomultiplier tubes. In the second method, line light illuminators and scan cameras are used to retrieve images of the defects. The last method uses an area light illuminator and frame cameras. The difference between these image acquisition methods is that frame and line scan cameras may not detect as much information as the flying spot scanning method does. [1, 16]

The design of the camera regarding pixel dimensions is contributing to the resolution limit of the AOI. In the case of large defects, many sensor pixels are covered. The image processing system programs an appropriate threshold and counts the number of pixels above the threshold. In the case of small defects, only a few sensor pixels are covered and some of the pixels can be only partially covered. In general, the defect must cover at least two pixels so that the defect can be detected. When choosing the camera, features presented in Figure 10 must be taken into account. Working distance (WD) is the distance between the lens of the camera and the inspected object. It changes according to the magnification. Smallest feature is the smallest feature of the object which is desired to be detected. Sensor resolution describes the minimum number of pixels needed to represent the inspected object. Depth of field is the maximum depth in the sample which remains in focus. Field of view (FOV) is the area which the camera can acquire during inspection. [17–19]

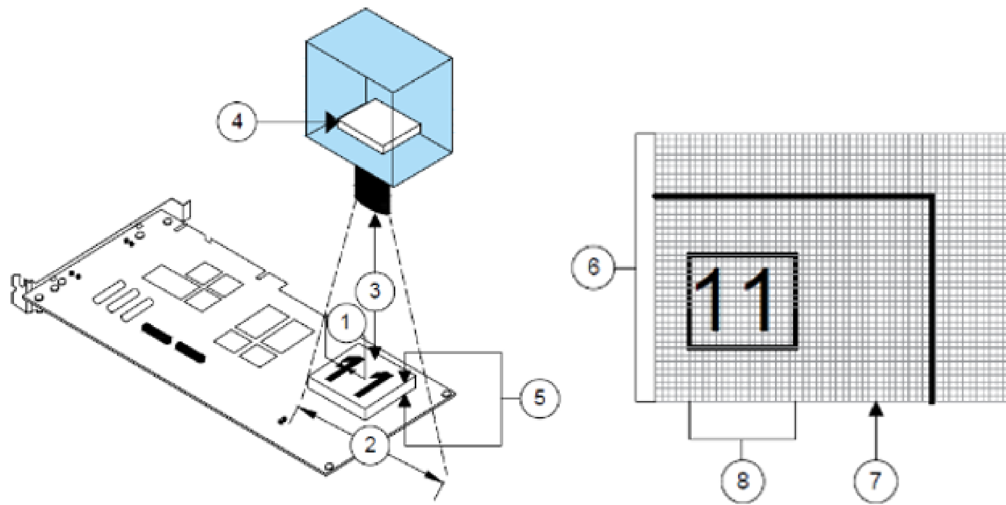

Figure 10. Features that should be taken into account when choosing the camera. The image was retrieved from [19] 1.) Resolution 2.) Field of view 3.) Working distance 4.) Sensor size 5.) Depth of field 6.) Image 7.) Pixel 8.) Resolution of the pixel

An equation for the required camera resolution can be derived if the FOV and smallest feature are known

$$\text{sensor resolution} = 2\left(\frac{\text{FOV}}{\text{smallest feature}}\right). \tag{4}$$

The resolution of the sensor corresponds to the resolution of the image. The resolution of the image is the number of pixels, rows and columns, in the image [18]. Another important equation which determines the lens specifications is the equation for focal length

$$\text{FL} = \frac{\text{SZ} \times \text{WD}}{\text{FOV}}, \tag{5}$$

where SZ is the image sensor area. In addition, frame rate should be also considered particularly in mass production AOI applications. Frame rate is the rate of consecutive images captured or displayed. [19]

There is also different options for the image sensors in AOI equipment. The image sensor can be charge coupled device (CCD) or complementary metal oxide semiconductor (CMOS). In addition, the sensor can be in grayscale or colors. The applications for the sensor differ from each other. CCD sensors can be more effective for precision measure-

ment as they have better linearity and signal-to-noise ratio (SNR). Therefore, they are used in inspection tasks related to the linear transformation of pixel gray level. CMOS sensors, on the other hand, are better in signal dynamic range and sampling speed. They are more suitable for surface defect inspection in which strong reflective or scattering light occurs. Grayscale sensors decrease the quantity of the data while losing the color information of defects. The data is therefore transmitted and processed faster, but the color information of the defects is lost. The color sensors can be important in defect determination and classification. [1, 16]

The entire system including the motion control, illumination modules, image acquisition, and inspection recipe programming is controlled by the software. The motion control moves either the inspected object or the hardware. In case of a wafer inspection, moving the wafer itself is faster but this can cause unwanted movement into the detailed structures of the patterned wafer interfering the inspection. Instead, the hardware is usually moved relatively to the wafer so that the handling of the wafer is easier and the inspection is more stable. In addition, the software may have a variety of unique features such as algorithms which may perform additional analysis on the data like image classification or nuisance reduction. [10]

Just as hardware plays a part in the capability and quality of the AOI, so does the inspection recipe programming play an important role, too. The programming is all about finding the balance in which the inspection is sensitive enough to catch all the defects of interest (DOI) but not too sensitive so that the detection of nuisances is in an appropriate level. The sensitivity of the inspection has an effect on the stability. Very sensitive inspection has a tendency to be unstable for process variations. The quality and suitability of inspection recipes can be measured by many different metrics. The most basic metric is the overall defect count. If the defect count is very low, the inspection might not be sensitive enough. Correspondingly, high defect count can indicate that the inspection is too sensitive. Other traditional metrics are nuisance defect and DOI rate. The nuisance rate shows the proportion of nuisance defects in the overall defect count. DOI rate shows the proportion of DOI's in the overall defect count. Low nuisance and high DOI rates indicate that the inspection performs well. Gauge repeatability and reproducibility (GAGE R&R) measurements can give perspective of the inspection recipe stability in repeated inspections. Repeatability measures how well the outcome of a measurement can be reproduced in unchanged conditions. Respectively, reproducibility measures how well the outcome can be reproduced in changing conditions. Throughput measures the time of the inspection. Very sensitive inspection can take a long time. Therefore applying a very sensitive inspection into mass production might not be beneficial. [20]

4 DEFECT DETERMINATION

4.1 Definition of a defect

Defect is an imperfection which can originate from the process, equipment, and manual handling, for example. The defects are detected and evaluated by their features during AOI, but the determination of whether the defect is a real defect or a false defect is usually left out for human verification. A wafer map indicating the defective elements can be constructed from the defect locations reported by the AOI. Defective elements can occur in random manner, clusters, or systematic patterns. Clusters and patterns on the wafer typically indicate that the manufacturing process has anomalies such as uneven processing temperature or photo mask misalignment. [4]

Stiction and breakage of suspended parts are common defect types for surface micromachining. Example defect images taken with scanning electron microscope (SEM) are shown in the Figure 11. Stiction occurs when the element is removed from the liquid etchant. Capillary forces keep the suspended part stuck while the suspended part is pulled towards the substrate surface. It can also result from over-range input signals or electromechanical instabilities during operation. The surfaces are brought into contact and they remain stuck until the over-range voltage is disappeared. In addition, particles can affect to the functionality of the die in many ways. The particle can mask the lithography process resulting in unetched structures, or the particle can move to the cavities and prevent the movement of the mass. There can also be some roughness on the bottom or on the edges of the cavity resulting in defect images which show a difference in the cavity shadow. Sputtering and thin film processes can lead to spot-like residues. Scratch is also a typical defect which can originate anywhere from the process, equipment, and material handling. [4, 21]

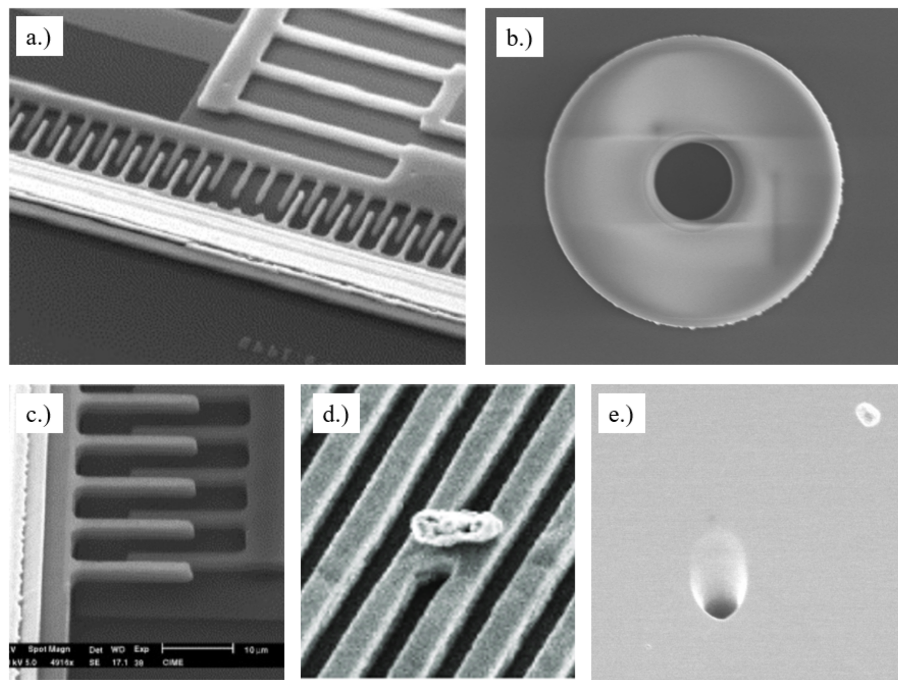

Figure 11. Example SEM images of common defect types seen on surface micromachined elements. Image a.) presents a breakage of a suspended part [21]. Image b.) is a resist drop from lithography process. Example of stiction is shown in image c.) [21]. Particle masking etching process is shown in image d.) [22]. Image e.) is a hole in silicon wafer.

4.2 Detection

The defect detection and image formation is a combination of diffraction and interference. The light from the illuminator is diffracted by the sample. The diffracted rays of light are collected by the objective lens, and focused in the image plane. A contrast image is formed by the recombination of light waves, inter alia interference. The recombination is affected by the properties of waves such as amplitude, wavelength, and phase difference. The amplitude of the resultant wave from the recombination is decreased (destructive interference) or increased (constructive interference). In the case of MEMS elements, the surface imperfections (defects) cause the scattering of light. The defect topography determine the scattering distribution which is described as scattered radiance as a function of scatter angle. No general conclusions about the scattering distributions for different defects cannot be made, because even same defect types can have different scattering distributions. [11, 17]

So, the image of a defect is a diffraction pattern created by the interference in the image plane. Under high magnification, the pattern consists of a central spot, diffraction disk,

surrounded by a series of diffraction rings. The central spot is a result of disturbance in the electric field of the wavefront in the lens aperture due to electromagnetic wave passing trough small aperture. The radius of the central diffraction spot is related to the Rayleigh's Equation (3) presented in Chapter 3. Short wavelength and large numerical aperture results in smaller diffraction center point radius. [11]

The diffraction of light from a defect can be modeled by simple transparent diffraction grating which is a planar substrate containing numerous parallel linear grooves (Figure 12). When the spacing between grooves is close to the wavelength of the illumination, the light is strongly diffracted. If the grating is illuminated with monochromatic light from a point source, the bright diffraction center point and various higher-order diffraction spots are observed. The central diffraction point is composed of waves which do not diffract during transmission through the grating. The higher-order diffraction spots present the diffraction angles along which waves have emitted from the grating. The spots appear bright because the emitted waves are in the same phase and the interference is constructive. Respectively, the areas between higher-order diffraction spots are black because the waves are out of phase and the interference is destructive. [11]

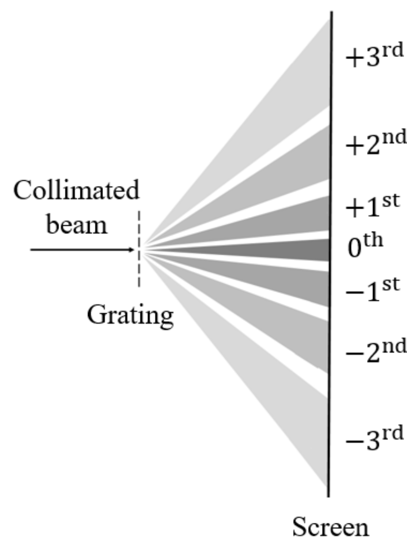

Figure 12. Diffraction grating can be used to model the basic principles of image formation. The grating is illuminated with monochromatic light which interacts with the grating resulting in diffracted rays of light. The bright central point is the 0th order of diffraction. Various higher-order diffraction points (1st, 2nd, 3rd, et cetera) are observed.

Ernst Abbe investigated and developed the theory behind image formation in the light microscope in Germany in 1873. Based on the Abbe's theorem, the image is formed by diffraction of light from the inspected object collected by the objective, and the interfer-

ence of both diffracted and nondiffracted light rays in the focal plane of the objective lens. The contrast of the image and the limitations in spatial resolution are determined by the interference between the diffraction central point and higher-order diffraction points. If the inspected object is similar to a diffraction grating, it can be stated that the image formation requires at least two orders of diffraction collected by the objective. If only the central diffraction point is collected by the objective, there is no interference. Therefore, image is not formed. As a conclusion, the more there is higher-order diffraction points collected by the objective, the better is the contrast, details, and information content of the formed image. [11]

Based on the Equation of resolution (3) and the theory by Ernst Abbe, the overall conclusion is that greater numerical aperture results in better resolution and contrast. However, this does not apply in all practical applications. In brightfield illumination, the numerical aperture should actually be small. This is because the aperture in brightfield illumination captures only the central point of diffraction. Darkfield illumination, in turn, benefits of a large numerical aperture, because the aperture collects the higher-order diffraction points. The contrast between the formed image of the defect and the background plays an important role in defect detection. [17]

The spatial resolution limit must be considered when interpreting the formed images. The shape of the objects whose size is greater than the resolution limit are resolved. On the contrary, the shapes of objects whose size is below the resolution limit appear as circular diffraction disks and have the same diameter, the resolution limit, despite their actual sizes and shapes. Based on this, objects whose size is below the resolution limit can be detected but their actual diameters are not resolved. [11]

Meanwhile diffraction and the wave properties of light determine the diameter of the diffraction disk of a point object, depth of field determine the thickness of the diffraction disk along the z-axis. It is determined by the physical and geometrical optics, lens aberrations, and magnification. Mathematically depth of field, Z, can be expressed as

$$Z = n\lambda \mathrm{NA}^2, \tag{6}$$

where n is the refractive index of the medium, λ is the wavelength of light, and NA is the numerical aperture. Depth of field describes the thickness of optical section along z-axis in which the object is focused in the object plane. Depth of focus, in turn, describes the thickness of the image plane. [11]

4.3 Image processing

Whereas diffraction and interference detect the defect from the inspected object, it is left for machine vision to detect the defect from the image. The first steps in visual defect detection can be dated back to 1973 when two-dimensional nonlinear logical filtering was applied to detect defects in PCBs. The tasks related to defect detection can be divided into classification, localization, and segmentation. Image processing is required to extract enough features from the images so that the information about the defect can be understood. The whole system of image processing is sketched in Figure 13. [14]

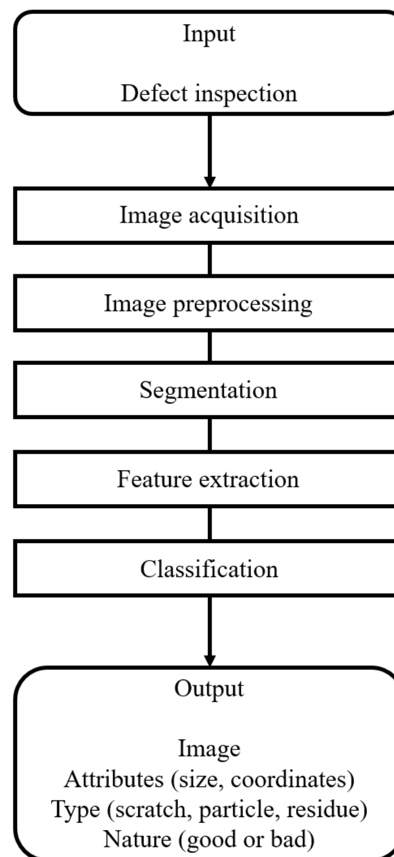

Figure 13. Diagram of the image processing system. The input is the defect inspection from which the image is acquired. The image is preprocessed so that segmentation, feature extraction, and classification can properly understand the information in the image. The system outputs information about the defect such as the image, attributes, type, and nature in terms of good or bad.

In image acquisition, an image of a certain area on the MEMS element is acquired. The image can be analysed with different defect determination methods such as referential, non-referential, and the combination of both methods. In the referential method, the im-

age is compared to a reference image of a healthy MEMS element. In the non-referential method, the determination of a defect is based on design rules to see if the image of the MEMS element is within the predefined limits or not. The last method, hybrid method, is a combination of the first two methods and is therefore more complex. [23]

In referential method, there is a reference image presenting the healthy structure of a full or partial element. A test image, resulting from the inspection of an element on a wafer, is compared to the reference image. These images are subtracted, meaning that the pixel values of these two images are subtracted. As a result, a third image presenting the differences in the pixel values, is formed. If there are no differences between the reference and test image, the difference image is black as the pixel values are zero. Otherwise, the pixel values indicate whether the difference is caused by additional material or missing material defects. As an ideal example, additional material defects are seen as negative pixels and missing material defects are seen as positive pixels. Overall, the image subtraction method is a combination of acquisition, processing, alignment, and subtraction. [23, 24]

In image preprocessing, the images are enhanced by masking, filtering, or geometric transformations so that the images contain less noise and have better contrast. Images are preprocessed so that segmentation, feature extraction, and classification algorithms can better understand the images. Image preprocessing uses the methods of spatial and frequency domains in which Fourier transform is typically used to convert the signal from spatial domain to frequency domain. In frequency domain, wavelet transforms are used. The most general algorithms related to preprocessing include histogram equalization, Median filter, Gaussian low-pass filter, and mathematical morphology. In addition, the image can be masked so that the region of interest can be defined. With this masking operation, the inspection time is reduced because the following operations such as feature extraction is only applied to this region of interest instead of the whole image. Geometric transformation calculates the projection of the pixels in the region of interest onto another space correcting the geometric distortions. [14, 19, 23, 25]

Segmentation groups the image into several homogeneous regions based on different characteristics. The objective is to define categories for each pixel values. There are three main classes for image segmentation methods: region-, edge-, and specific-theory-based methods. Examples of region-based segmentation methods are threshold segmentation, regional growth, clustering, and splitting and merging. Edge-based methods include first-order and second-order differential operator methods. Wavelet transform and mathematical morphology belong to specific-theory-based methods. [14]

Threshold segmentation uses grayscale thresholds which divide the pixels of the image into separate groups. It is simple and widely used but dependent on the choice of the threshold. Regional growth uses growth criteria to combine small similar regions into larger regions. However, it cannot be used for real-time detection because of the dependency on initial condition selection and large calculation. Clustering segments the feature space and uses the results to map the image space. Splitting and merging is similar to regional growth method. The non-uniformities of a region is used to to divide the image into smaller areas which can be later merged into larger areas by combining similar areas. It is dependent on the split and merge criteria. First-order differential operator is based on the discontinuity of the characteristics in the image. By applying an algorithm, the discontinuities can be used to localize the boundaries between the object and the background. Second-order differential operator, on the other hand, uses operators to localize the boundary by determining the zero-crossing point of the second derivative of the image grayscales. First-order differential operator is fast and simple but the positioning can be inaccurate. Second-order differential operator is accurate but sensitive to noise. [14]

Feature extraction processes the pixels in the image. It extracts the information and maps the differences to a lower-dimensional feature space so that the data can be compressed and the recognition can be more efficient. The features of the defect extracted can be grayscale and grayscale difference statistical characteristics. In addition, the shape and size of the defect can be extracted resulting in information about the lines, rectangles, area, and perimeter, for example. Feature extraction methods based in statistical characteristics are simple, effective, and widely used. Histograms are typical examples of this method. However, these take into account only the probability of the grayscale level of the image, ignoring the spatial distribution of the pixels. Grey-level co-occurence matrix calculates the spatial correlation properties of the grayscale to describe the texture with characteristics such as correlation, contrast, energy, and entropy. To reduce the computation time of the inspection algorithm, feature selection such as principal component analysis, is applied to the extracted features so that only the most important features contributing to the classification can be chosen. [14, 19]

The extracted features are used in classification. The output of the classification can be binary or multi-class. Binary classification classifies the defect as good/bad or pass/fail. Multi-class classification results in more than two group classification which can give insights of the defect type, for example. The algorithm used in classification determines whether the classification is rule- or learning-based. Rule-based classification is widely used due to the simplicity. It uses conditional statements and Boolean rules to classify the image as good or bad. However, rule-based classification has no capability to learn due

to which it's accuracy is dependent on successful feature extraction and the selection of suitable statements and rules. A common example of rule-based classification is thresholding in which threshold values are set for the extracted features. If threshold values are exceeded, the image can be treated as defective. [19]

Learning-based classifiers, inter alia machine learning classifiers, are capable to learn input and output correlations which can be used in classification and regression. They can be divided into supervised and unsupervised algorithms from which supervised machine learning algorithms are most commonly used. Examples of supervised machine learning algorithms are decision trees, k-nearest neighbor, support vector machines (SVM), and convolutional neural network (CNN). [19]

Decision tree classifier uses a tree resembling structure to describe relationships between defect features to make decisions. It is similar towards rule-based classification but the difference is that decision tree can learn itself. Nearest neighbor classifier operates with the selected k-value representing the nearest data points in the feature space that are closest to the points to be classified. The basic principle is that the estimated mean value of the k nearest neighbors is the output value for the predicted data point. SVM determines a hyperplane to two or higher dimensional problems which separates two classes from each other. If the classes cannot be perfectly separated, the hyperplane is set in a way that the misclassification is minimized. The logic of these algorithms is visually explained in Figure 14. [19]

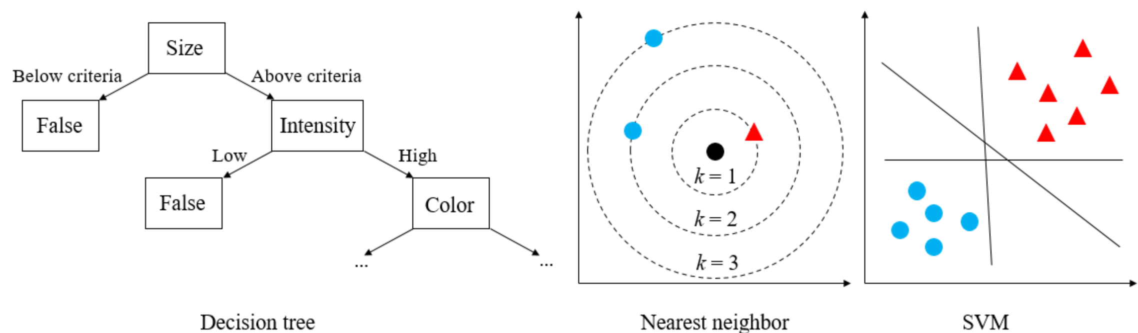

Figure 14. The logic of supervised machine learning algorithms. Decision tree has a tree-like structure with nodes indicating simple decision rules. Nearest neighbor determines the class for the unknown data point by its neighbors. If $k = 1$, the class would be determined by the red triangle. If the $k = 3$, the class would be determined by the blue circles. SVM determines the optimal hyperplane to separate two classes from each other.

CNN is a supervised deep learning algorithm whose deep neural network architecture

is especially capable in image processing and pattern recognition. It has convolutional, pooling, and fully connected layers as shown in Figure 15. First, the convolutional layer processes the input and outputs a feature map to the pooling layer. Pooling layer reduces the dimensionalities of the feature map. Finally, the fully connected layer maps the input to a feature vector for classification. Deep learning has attracted attention in defect detection algorithms because it can simultaneously perform both feature extraction and defect classification tasks. The functionality is based on training data from which the algorithm trains itself. The majority of deep learning defect detection algorithms are based on deep CNN. [26]

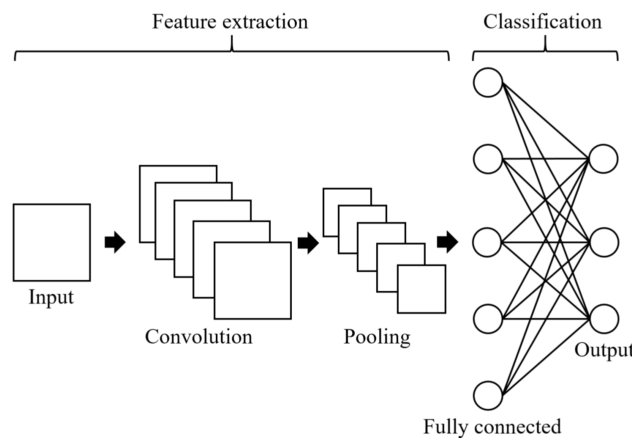

Figure 15. The structure of CNN.

Unsupervised machine learning algorithms such as clustering, cellular neural network, and self-organizing map (SOM), are used to find patterns and classifications in datasets. Clustering can be partitional in which the majority of the methods are based on an iterative optimization of a criterion function, or it can be hierarchical where the objective is to find a hierarchy for the clusters. Cellular neural networks are nonlinear dynamic systems which consist of large array of processing units. The processing units are only connected to the neighbor units in the neighborhood. SOM produces a low dimensional representation, a feature map, of high dimensional data while conducting similarity relations for the data. It is a single layer neural network with units locating in an n-dimensional grid which uses lateral interactions among neurons to construct a semantic map in which similar patterns are mapped close to each other. Machine learning classifiers are powerful and give more information compared to the rule-based classifiers but there can be problems with data overfitting and imbalance. Overfitting and imbalance are related to the lack of training data. If there is not enough training data, the model can be overfitted. If certain defects have more training data than other defects, the model can be imbalanced. [19, 27, 28]

5 DETECTION CAPABILITY IMPROVEMENTS

To improve the detection capability in optical inspection, the Rayleigh's resolution limit discussed in Chapter 3 should be exceeded. Therefore, small wavelength and large numerical aperture should be used to achieve better resolution. According to the Table 1, changing from visible light to ultraviolet or x-ray light, smaller wavelengths can be taken into use. Respectively, smaller defects can be detected.

By changing from automatic optical inspection into automatic electron beam inspection, the resolution limit can be decreased down to 1 nm. Electron beam inspection would improve the sensitivity limitations regarding optical inspection. However, the throughput with electron beam inspection is worse compared to optical inspection due to which it is not applied into manufacturing use. The throughput of the electron beam inspection can be improved by using massively parallel electron beams instead of a single electron beam. However, the application of multiple electron beams is not yet applicable as there are problems with alignment and image stitching which arise from the interactions between electron beams and the size of the electron beam pitch. [29]

A critical parameter in terms of production AOI equipment is the throughput. Inspecting the whole wafer with the smallest possible wavelength and field of view might be too time consuming. Therefore, breaking the inspection into multiple tests would be beneficial. For the element areas which do not have small structural details or are not sensitive to defects, could be inspected with less sensitive inspection recipe characteristics. For example, bigger wavelength and smaller magnification could be used. On the contrary, for the element areas with detailed or moving structures, smaller wavelength and higher magnification could be used to detect defects with small sizes. By dividing the inspection into multiple tests, the recipe characteristics can be optimized for different element areas, and the inspection time can be reduced.

In addition to the resolution limit, SNR and contrast have a great impact on the defect detection, too. SNR and contrast depend on the wavelength used and the material of the defect and the background. More precisely, the refractive index, reflectivity, and topography of both the defect and the background have a great impact to the SNR and contrast. Therefore, it might not be beneficial to choose the smallest wavelength possible for the inspection. Typically, materials have different reflectivity at the majority of wavelengths, but at some specific wavelengths, the reflection properties are similar. In these intersection points, the image contrast and the SNR of the defect scattering signal is poor. Correspondingly, if the selected wavelength is far away from the intersection point, the

defects are more clearly separated from the background. So, rather than focusing only on the resolution, the focus should be shifted towards finding the wavelength at which both contrast and resolution are optimal. [29]

The future trends of AOI are mainly related to defect detection algorithms and exceeding the resolution limit with new detection technologies. As the traditional brightfield optical inspection does not fulfill the resolution requirements in the future, substituting technologies must be developed. For example, critical dimension SEM, critical dimension small-angle x-ray scattering, scatterometry, 3D atomic force microscope, and transmission electron microscopy could be taken into account. Moreover, these techniques can be combined to hybrid methods to merge the capabilities of the methods. It is important to consider throughput, resolution, contamination, and possible damage when developing new technologies. [30]

Machine vision is the workhorse in defect detection algorithms. In the future, the focus should be in improving the problems related to machine vision defect detection. Machine vision requires high-dimensional feature space and a large amount of data due to which the speed of the image processing is slow. With complex geometry features, the throughput of real-time defection is weak. In addition, the dependence of the defect detection on the image acquisition system should be minimized. [14]

As deep learning has developed rapidly in recent years, defect detection algorithms based on deep learning have attained attention. Traditional machine learning algorithms rely on manually designed features, such as color and geometry features, which are used in defect classification. Therefore, the classification is not flexible and has a poor adaptability. On the contrary, deep learning is more flexible and accurate defect classification method. The defect classification can be obtained straight from the input image without the need of preprocessing. Downside is that it requires a large labeled data set so that the fitted model is the most optimal. Collecting a large dataset can be slow and expensive. To overcome data acquisition problems, future research should be focused on weak unsupervised learning methods. [2, 10, 14]

Throughput is an important parameter in production AOI applications. The amount of data involved in the inspection is large and becomes larger when more sensitive inspections are used. The main factor influencing the throughput of the inspection is the image processing system. The image processing and detection algorithms should be optimized such that they are accurate yet fast. Computers with high-performance as well as considering quantum computing are expected to improve the throughput of the inspection. [14]

6 EXPERIMENTS

6.1 Experiment wafers

The wafers used in the experiments were programmed defect wafers. Programmed defect wafers have intentionally created defects on the surface of the wafer. The performance and capability of the AOI equipment could be determined with the help of known programmed defect locations. For a rough estimation of the resolution and repeatability of the AOI equipment at Murata Electronics Oy, an 8 inch programmed defect wafer provided by the equipment manufacturer was used. The surface material used to pattern the defects was chromium. So, some areas on the wafer had silicon and chromium stacked on top of each other, and some areas had only silicon as a surface material. For more accurate resolution and repeatability measurements, 12 wafers with 6 inch diameter from the element manufacturing of Murata Electronics Oy were used. The surface materials in wafers 1 to 6 was silicon and silicon dioxide. In wafers 7 to 12 the surface material was silicon. The experiment wafers are listed in Table 2.

Table 2. Wafers used in the experiments.

<table>
<tr><th>Manufacturer</th><th>Lot ID</th><th>Wafer ID</th><th>Details</th></tr>
<tr><td>Equipment manufacturer</td><td>No ID</td><td>6</td><td>Step 2</td></tr>
<tr><td rowspan="2">Murata Electronics Oy</td><td>1</td><td>1-6</td><td>Step 2</td></tr>
<tr><td>2</td><td>7-12</td><td>Step 1</td></tr>
</table>

The process flow of Murata Electronics Oy defect wafers had some minor changes compared to the normal process flow. In the lithography process where the desired element layout is patterned onto the wafer, a defect mask instead of the normal product mask was used. With this, the programmed defects could be patterned to the wafer. Later during the etching process, only one etching chamber was used to avoid the variation between etching chambers. Six defect wafers were processed until the etching process. Rest of the wafers were etched. In total, there were two types of defect wafers - wafers which were only patterned and wafers which were patterned and etched. In the Table 2, patterned wafers are denoted as step 2 wafers. Respectively, patterned and etched defect wafers are denoted as step 1 wafers.

6.2 Inspection recipes

The determination of the AOI equipment resolution, repeatability, and accuracy was divided into two different approaches in terms of inspection recipe creation:

1. Recipe version 1
   Inspection recipe with less sensitive characteristics
2. Recipe version 2
   Inspection recipe with sensitive characteristics.

In the first approach, the wavelength of the inspection light and the values for threshold parameters were larger than in the second approach. In the second approach, the wavelength of the light source was decreased as it increases the resolution according to the Rayleigh's Equation (3). Also, the threshold parameters were decreased to detect more defects even though this similarly increases the detection of nuisances. For both approaches, every magnification of the equipment was tested to investigate their capabilities separately.

The AOI equipment was loaded with wafer boxes containing the programmed defect wafers. For recipe version 1, white light was selected. Blue light was selected for the recipe version 2. Optimal light levels were trained for the desired inspection channels. Test inspections revealed that DF channel was not capable to detect programmed defects on the defect wafer provided by the equipment manufacturer. This was expected as the surface of the programmed defects were approximately at the same level as the surface of the wafer. Therefore, only BF channel was used. For the defect wafers provided by Murata Electronics Oy, BF and DF channels were used.

Then, the areas on the element to be inspected were drawn as care areas. Only the areas that contained programmed defects were drawn to minimize the detection of nuisances. For each care area, an appropriate threshold was tested and defined by test inspections. The value of the threshold describes the limit by which the equipment determines if the detected difference in the defect image is significant enough to be defined as a defect. For recipe version 1, the goal was to find threshold values which minimize the detection of nuisance defects. For recipe version 2, the goal was to detect as much programmed defects as possible, even tough this increases the detection of nuisance defects.

Overall, the threshold values for recipe version 2 were about two units smaller than the threshold values in recipe version 1. In addition, the threshold values for DF channel were

two units larger than in BF channel. This is because DF is more sensitive to nuisances as the detection is based on scattered light. For the defect wafers provided by Murata Electronics Oy, it was assumed that the area of the programmed defects was not that small that 10X magnification would have required as sensitive thresholds as other magnifications. Therefore, the threshold values for 10X magnification were almost two times larger.

Finally, additional postprocessing criteria which filters out defects below certain defect bounding box area was added. For the defect wafer provided by the equipment manufacturer, no postprocessing criteria was used because the wafer contained small defects. For the defect wafers provided Murata Electronics Oy, no postprocessing criteria was added for 2X magnification because the resolution of 2X is the weakest. For 3.5X and 5X magnification, defects with defect bounding box area below 1.69 μm^2 were removed from the inspection results to reduce nuisances. Because the defect count resulting from the 10X magnification inspection was so high that the inspection was failed, the area criteria was increased to 5 μm^2. With this increase, the inspection could be performed successfully.

Wafer maps in the Appendix 1 show the distribution and density of the programmed defects detected on the wafer. There are wafer maps for every defect wafer, magnification, and recipe version. Respectively, stacked dies (elements), are presented in the Appendix 2. There are stacked dies for every defect wafer, magnification, and recipe version. There are also stacked dies separately for all defects and programmed defects only to see how much defects were detected overall, and how many of the defects detected were actually programmed defects. The defects are stacked on top of each other so that the distribution and density of the defects on one element can be seen.

6.3 Data

The datasets contain data from the defect wafer inspections conducted with the AOI equipment. Each dataset has data from 10 repeated inspections. One row represents one defect and columns represent defect attributes. For some rows, there is a defect image available. The datasets used in the data analysis are listed in the Table 3.

Table 3. Datasets retrieved from the experiments.

Recipe version	Wafer	Wafer ID	Magnification			
			2X	**3.5X**	**5X**	**10X**
1	Equipment manufacturer defect wafer	6	Dataset 1	Dataset 3	Dataset 5	Dataset 7
	Murata Electronics Oy defect wafer	1	Dataset 9	Dataset 11	Dataset 13	Dataset 15
		2	Dataset 17	Dataset 19	Dataset 21	Dataset 23
		3	Dataset 25	Dataset 27	Dataset 29	Dataset 31
		4	Dataset 33	Dataset 35	Dataset 37	Dataset 39
		5	Dataset 41	Dataset 43	Dataset 45	Dataset 47
		6	Dataset 49	Dataset 51	Dataset 53	Dataset 55
		7	Dataset 57	Dataset 59	Dataset 61	Dataset 63
		8	Dataset 65	Dataset 67	Dataset 69	Dataset 71
		9	Dataset 73	Dataset 75	Dataset 77	Dataset 79
		10	Dataset 81	Dataset 83	Dataset 85	Dataset 87
		11	Dataset 89	Dataset 91	Dataset 93	Dataset 95
		12	Dataset 97	Dataset 99	Dataset 101	Dataset 103
2	Equipment manufacturer defect wafer	6	Dataset 2	Dataset 4	Dataset 6	Dataset 8
	Murata Electronics Oy defect wafer	1	Dataset 10	Dataset 12	Dataset 14	Dataset 16
		2	Dataset 18	Dataset 20	Dataset 22	Dataset 24
		3	Dataset 26	Dataset 28	Dataset 30	Dataset 32
		4	Dataset 34	Dataset 36	Dataset 38	Dataset 40
		5	Dataset 42	Dataset 44	Dataset 46	Dataset 48
		6	Dataset 50	Dataset 52	Dataset 54	Dataset 56
		7	Dataset 58	Dataset 60	Dataset 62	Dataset 64
		8	Dataset 66	Dataset 68	Dataset 70	Dataset 72
		9	Dataset 74	Dataset 76	Dataset 78	Dataset 80
		10	Dataset 82	Dataset 84	Dataset 86	Dataset 88
		11	Dataset 90	Dataset 92	Dataset 94	Dataset 96
		12	Dataset 98	Dataset 100	Dataset 102	Dataset 104

6.4 Description of experiments

The experiments conducted for the datasets in the Table 3 are listed below:

1. Repeatability and resolution analysis
   Defect coordinates from the repeated inspections are clustered with query_ball_-point() function from cKDTree class, scipy.spatial library in Python 3.8. The objective was to determine the repeatability and resolution of the AOI equipment. Repeatability was calculated for every programmed defect. It was reported as a percentage which indicated how many of the repeated inspections had repeated the

defect detection. The resolution was measured as the smallest defect bounding box area in which the average repeatability was at least 90 %.

2. Accuracy analysis
   Median relative standard deviations are calculated for the defect attributes by grouping the results from the repeatability and resolution analysis. The grouping is done by the defect coordinates. The objective was to determine the accuracy of the AOI equipment in terms of the defect attributes. In other words, the uncertainty of the inspection was evaluated.

3. Difference image comparison for different wavelengths
   Test images are subtracted from reference images to retrieve the difference images. Defects are clustered by their coordinates to match the difference images. Difference images taken with different wavelengths are aligned, cropped, and compared to each other by calculating Structural Similarity Index (SSIM). The objective was to find whether the difference images retrieved with different wavelengths were similar. A big difference could indicate that some wavelength is inferior in terms of the defect image quality.

The quality of the experiments is evaluated with statistical methods. By calculating standard deviations and visually assessing the variability in the experiments, the uncertainty of the experiments can be measured.

6.5 Repeatability and resolution analysis

The repeatability and resolution of the AOI equipment was determined by comparing the programmed defect coordinates resulting from the repeated inspections. The repeating defect coordinates could be identified by clustering the datasets from the repeated inspections with cKDTree query_ball_point() function in Python 3.8. This function searches the nearest neighbors within a tolerance distance for given points. For example, if the number of nearest neighbors was 10, the detection of a defect was repeated in every inspection. Therefore, the repeatability for the detection of the defect was 100 %. If there were five nearest neighbors, the detection of the defect was repeated in half of the inspections. Thus, the repeatability was 50 %.

The effect of defect bounding box area to the repeatability of the defect detection was investigated. The hypothesis was that the smaller the defect, the smaller is the probability

of the detection of the defect to be repeated in repeated inspections. So, the defect bounding box area [µm^2] was plotted against repeatability [%]. The plotting was conducted for each dataset in the Table 3 so that every magnification and recipe version was taken into account. Figure 16 presents the relationship between defect bounding box area and repeatability for the defect wafer provided by the equipment manufacturer. The pink area shows the distribution between repeatability for each defect bounding box area. Black line shows the average repeatability for each defect bounding box area.

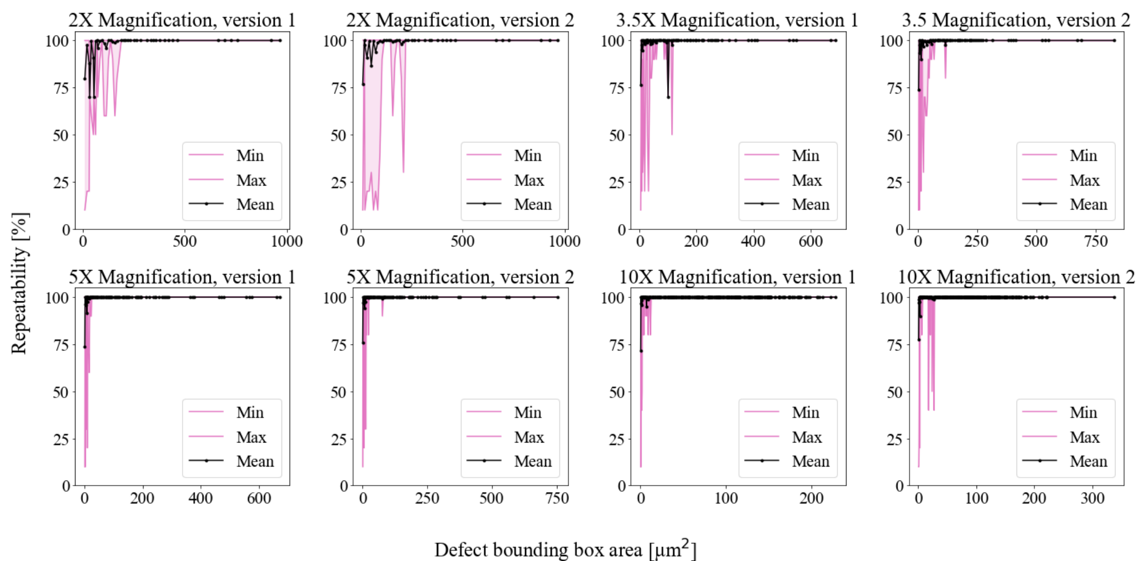

Figure 16. The affect of defect bounding box area to the repeatability of the detection of programmed defects. The figure shows the repeatability for each magnification and recipe version. The wafer inspected was the equipment manufacturer defect wafer.

A logarithmic trend between defect bounding box area and repeatability could be distinguished from the Figure 16. The hypothesis seems to be correct as the probability for a defect to be detected in repeated inspections is smaller with smaller defect bounding box areas. Also, the smaller the defect bounding box area, the more variation in the repeatability. A trend can be seen from the magnifications, too. The greater the magnification, the steeper is the curve at the beginning. So, the resolution and repeatability is better with higher magnifications. The variation in repeatability was more likely to be smaller at higher magnifications, too. The relative smallest defect bounding box areas which were detected with a 90 % probability are tabulated for each magnification and recipe version in Table 4. The result of 5X magnification with recipe version 1 characteristics was used as a reference to which other defect bounding box areas were scaled to.

Table 4. The relative smallest defect bounding box areas which are detected with a 90 % probability of the defect wafer provided by the equipment manufacturer. 5X magnification with recipe version 1 characteristics was used as a reference to which other defect bounding box areas were scaled to.

Recipe version	Magnification			
	2X	**3.5X**	**5X**	**10X**
1	8.33	2.40	1.00	0.29
2	7.29	2.40	1.17	0.34

Table 4 confirms the conclusions made from the Figure 16. The resolution decreases as magnification increases. Against the assumptions, the defect bounding box areas reported with more sensitive recipe characteristics (recipe version 2) were better only with 2X magnification. This can be due to the random variance between the inspections. There is also a possibility that the contrast and SNR between the defect and the background is better with white light than with blue light.

The analysis was repeated for the defect wafers provided by Murata Electronics Oy. The defect bounding box areas [μm^2] were plotted against repeatability [%]. In Figures 17, 18, 19, and 20 the results for the repeatability analysis are shown. The figures show merged results separately for recipe versions and magnifications. The distribution of repeatability is visualized with pink color interpreting the minimum and maximum for repeatability. The average repeatability is shown with a black line. Snippets from the beginning of the x-axis are embedded in each figure to interpret more clearly the logarithmic trend.

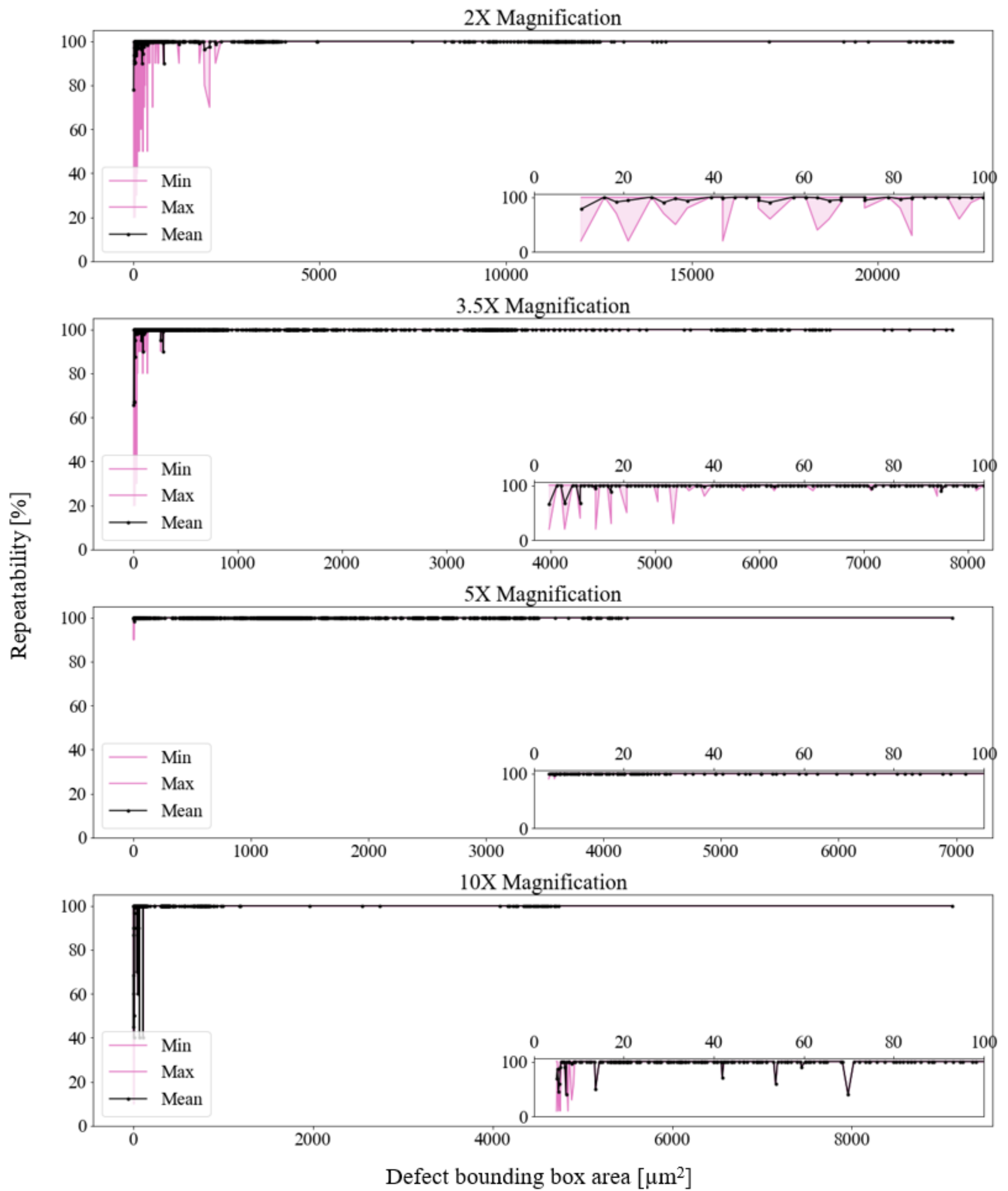

Figure 17. The affect of defect bounding box area to the repeatability of the defects detected. The figure shows the results individually for each magnification. Snippets from the beginning of the x-axis interpret more clearly the logarithmic trend at the beginning of the curve. The data used in the plotting is from the repeated inspections of step 2 wafers provided by Murata Electronics Oy. The wafers were inspected with recipe version 1.

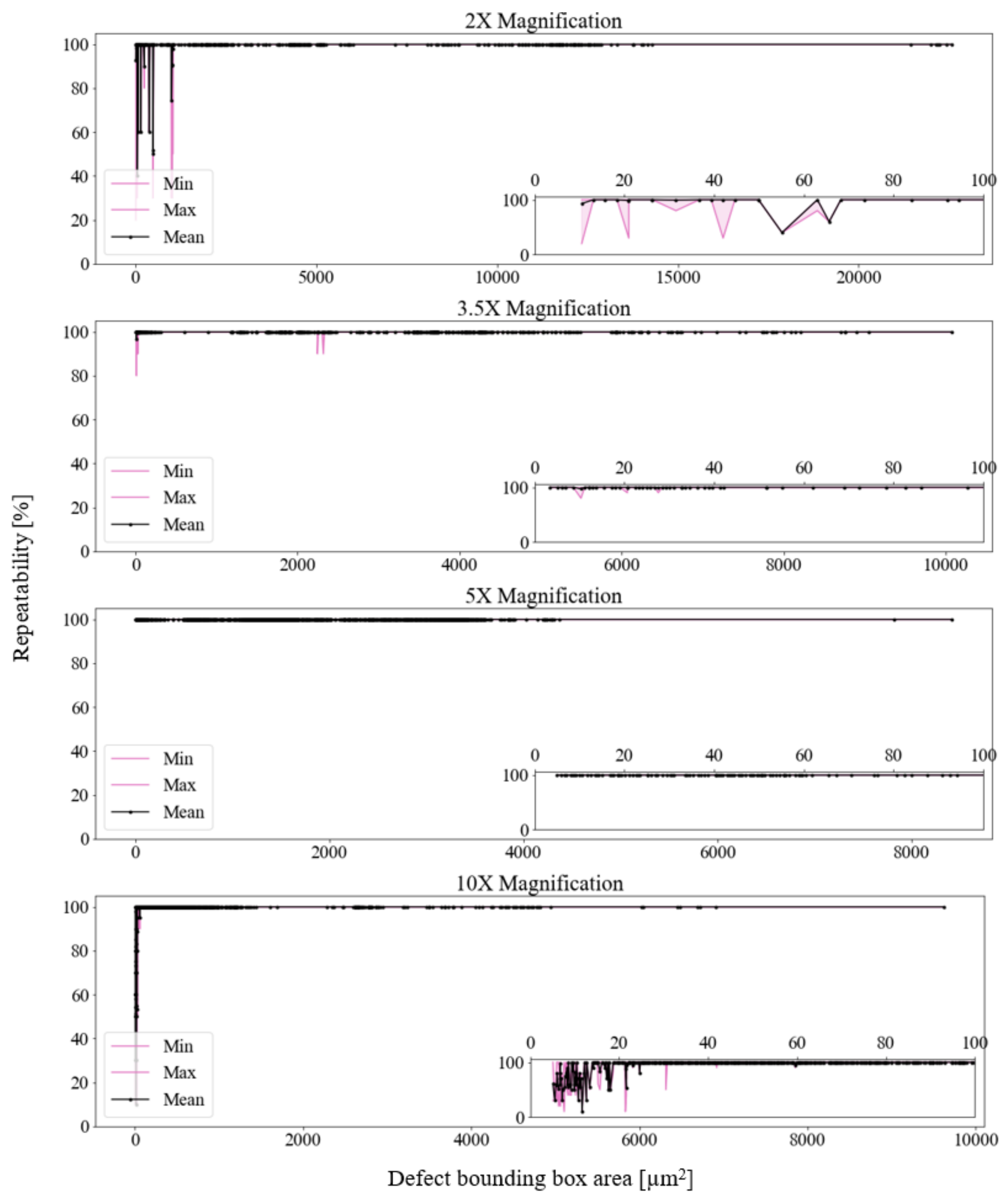

Figure 18. The affect of defect bounding box area to the repeatability of the defects detected. The figure shows the results individually for each magnification. Snippets from the beginning of the x-axis interpret more clearly the logarithmic trend at the beginning of the curve. The data used in the plotting is from the repeated inspections of step 2 wafers provided by Murata Electronics Oy. The wafers were inspected with recipe version 2.

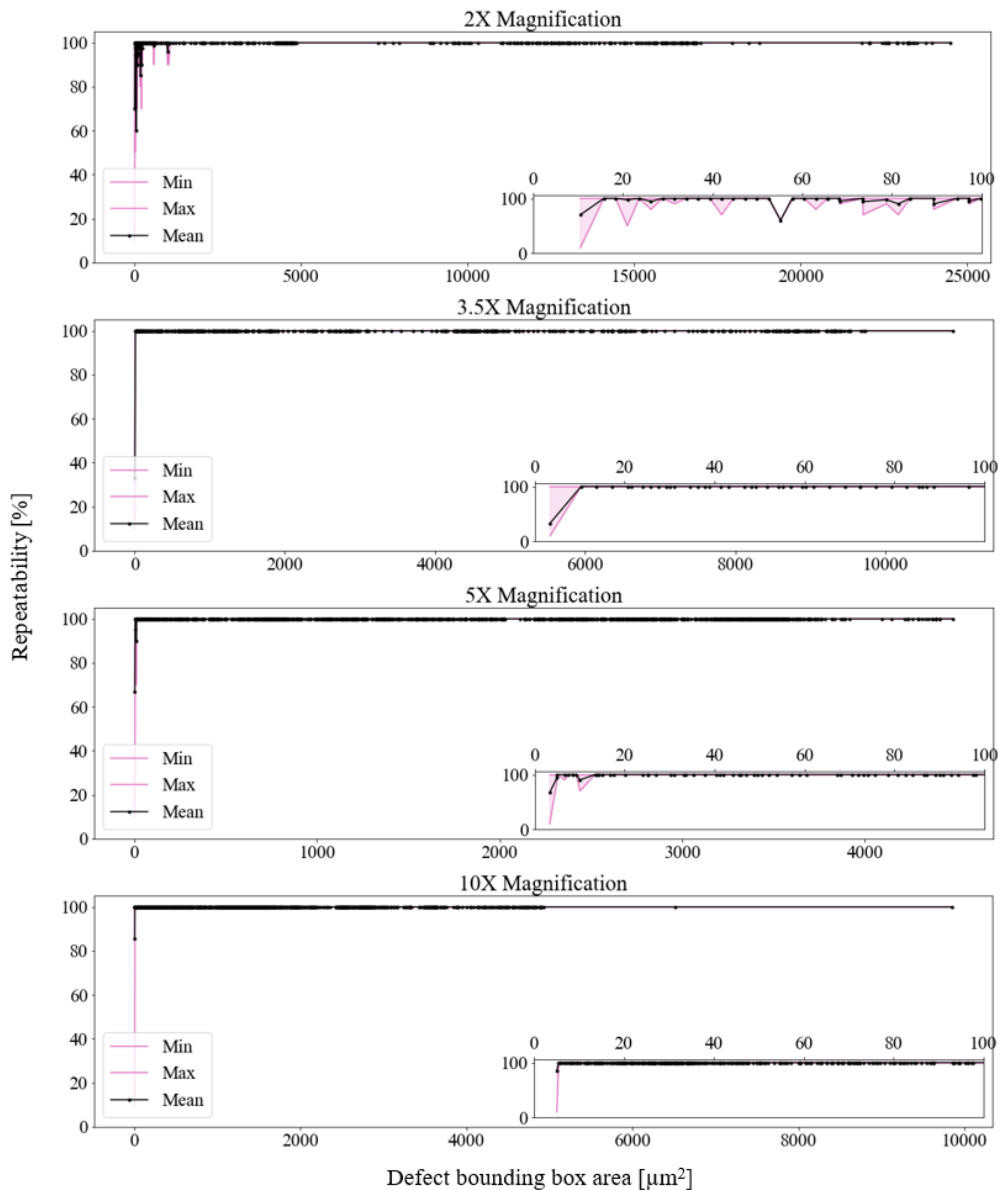

Figure 19. The affect of defect bounding box area to the repeatability of the defects detected. The figure shows the results individually for each magnification. Snippets from the beginning of the x-axis interpret more clearly the logarithmic trend at the beginning of the curve. The data used in the plotting is from the repeated inspections of step 1 wafers provided by Murata Electronics Oy. The wafers were inspected with recipe version 1.

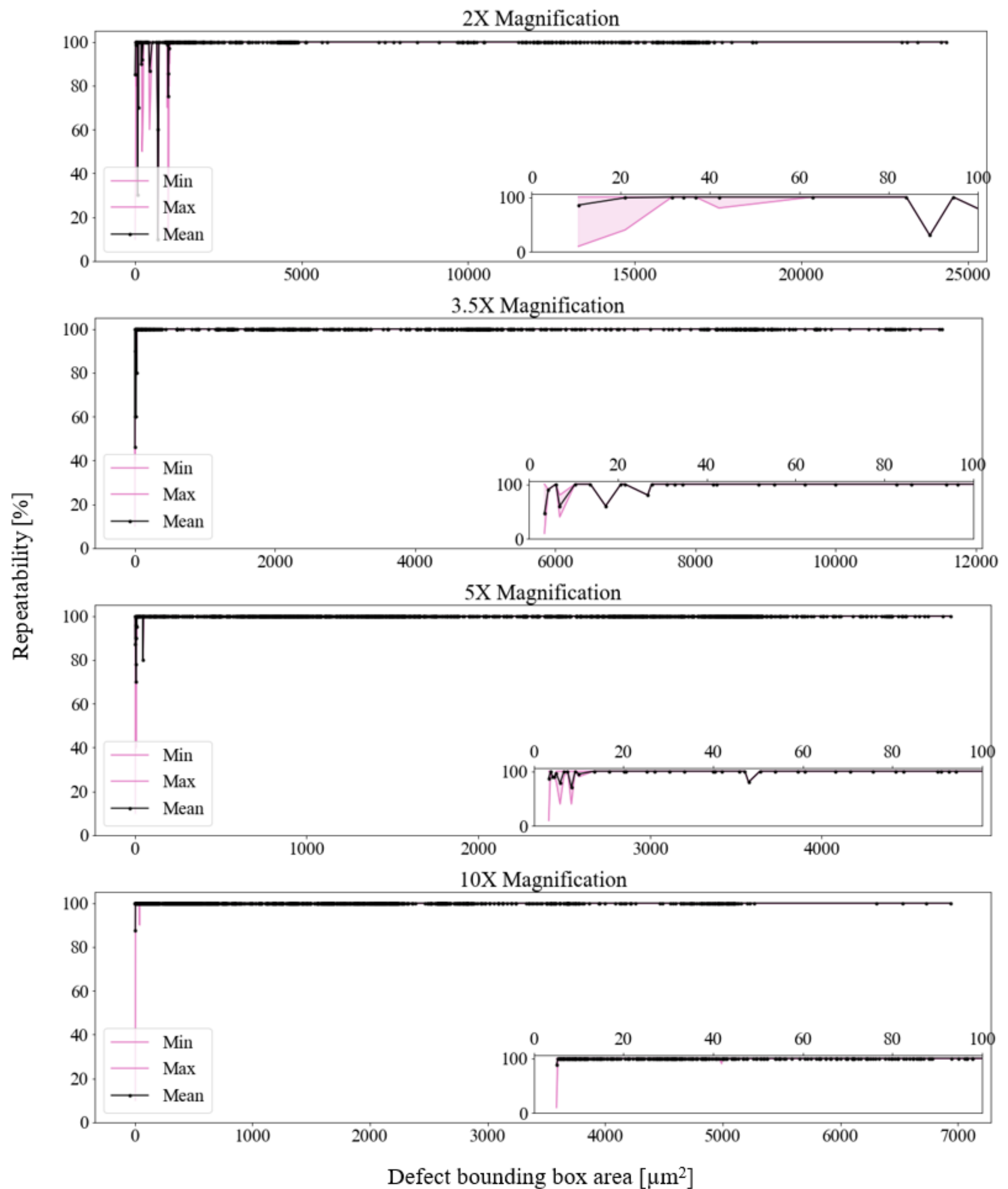

Figure 20. The affect of defect bounding box area to the repeatability of the defects detected. The figure shows the results individually for each magnification. Snippets from the beginning of the x-axis interpret more clearly the logarithmic trend at the beginning of the curve. The data used in the plotting is from the repeated inspections of step 1 wafers provided by Murata Electronics Oy. The wafers were inspected with recipe version 2.

Based on the Figures 17, 18, 19, and 20, a similar trend as seen in the repeatability results of the equipment manufacturer defect wafer (Figure 16) can be detected. The trend is logarithmic with a steep curve at the beginning. The snippets from the beginning of the x-

axis have in some cases high variation which can be due to the differences between wafers. With step 2 wafers, the variation seems to be less with recipe version 1 characteristics. The same conclusion applies for the step 1 wafers, too. The variation in repeatability is greater with step 1 wafers than with step 2 wafers. The difference can be explained by the wafer surface material. Step 2 wafers were mostly covered with silicon dioxide thin film whereas the surface of step 1 wafers was silicon. These surface materials have different reflection and absorption properties which affect to the defect detection. In addition, the contrast might be better with silicon dioxide thin film because the color of the defect is probably different than the color of the silicon dioxide thin film. The difference can be also explained with etching. Etched defect wafers (step 1 wafers) have cavities and probably more wafer-to-wafer variation. The relative smallest defect bounding box areas which are detected with a 90 % probability are tabulated in Table 5. Result for wafers 7-12 inspected with 5X magnification and recipe version 1 characteristics was used as reference to which other results were scaled to.

Table 5. The relative smallest defect bounding box areas which are detected with a 90 % probability of the defect wafers provided by Murata Electronics Oy. Result for wafers 7-12 inspected with 5X magnification and recipe version 1 characteristics was used as reference to which other results were scaled to.

Recipe version	**Wafer**	**Magnification**			
		2X	**3.5X**	**5X**	**10X**
1	1-6	2.53 ± 0.35	0.89 ± 0.05	0.50 ± 0.00	0.88 ± 0.04
	7-12	3.12 ± 0.29	1.54 ± 0.24	1.00 ± 0.12	0.88 ± 0.06
2	1-6	1.56 ± 0.15	0.51 ± 0.00	0.94 ± 0.09	1.01 ± 0.05
	7-12	2.34 ± 0.78	1.22 ± 0.81	0.56 ± 0.11	0.78 ± 0.05

For the step 2 wafers, it seemed that the best resolution is achieved with recipe version 2 characteristics. However, the resolutions obtained with 5X and 10X magnifications are actually worse with recipe version 2. Perhaps, recipe version 1 characteristics are actually better in achieving smaller resolution. The contrast of the defect images and the SNR between the defect and the background may be better with white light. The difference is seen with higher magnifications only because the overall capability is better and deviation is smaller. The deviation in resolution is smaller with recipe version 1 characteristics as could be seen in Figures 17 and 18. For the step 1 wafers it seems that the best resolution is achieved with recipe version 2 characteristics. As noticed from the Figures 19 and 20, the deviation in resolution is smaller with recipe version 1 characteristics. Again, the resolution decreases as the magnification increases. For step 2 and step 1 defect wafers, 10X magnification had worse resolution than 5X magnification. These anomalies can

result from the thresholds explained in Section 6.2. Recipes using 10X inspection had almost two times bigger thresholds compared to recipes using other magnifications.

Because the repeatability results of the equipment manufacturer defect wafer had so much variation, the repeatability analysis was divided between logic and array care areas to see if there was any differences. Figure 21 shows the affect of defect bounding box area to the defect repeatability for logic care area, magnification and recipe version. Similarly, Figure 22 presents the relationships for array care area.

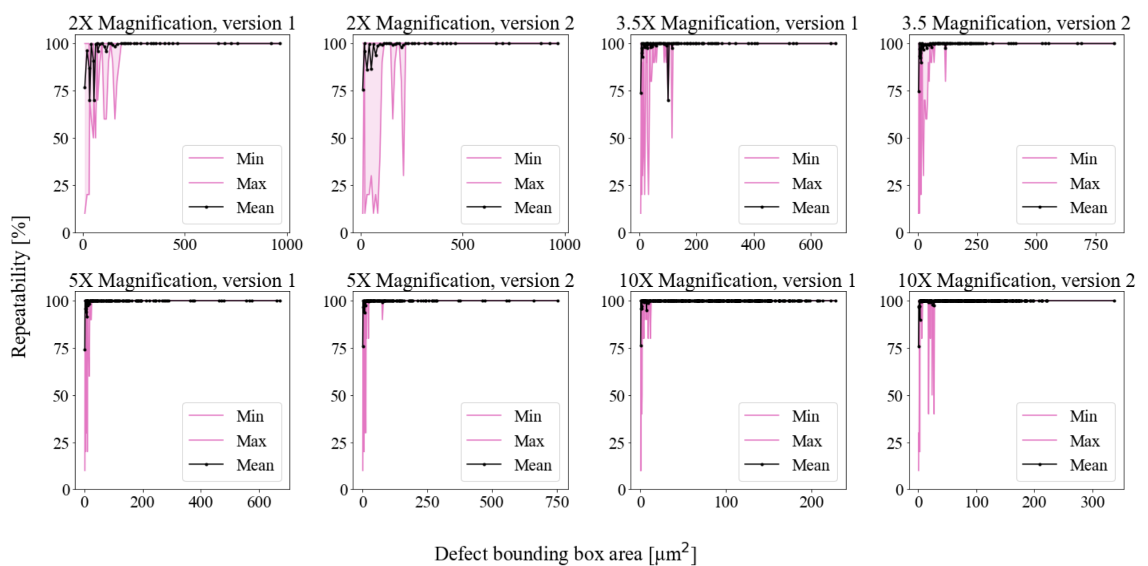

Figure 21. The relative smallest defect bounding box areas which are detected with a 90 % probability in logic care area.

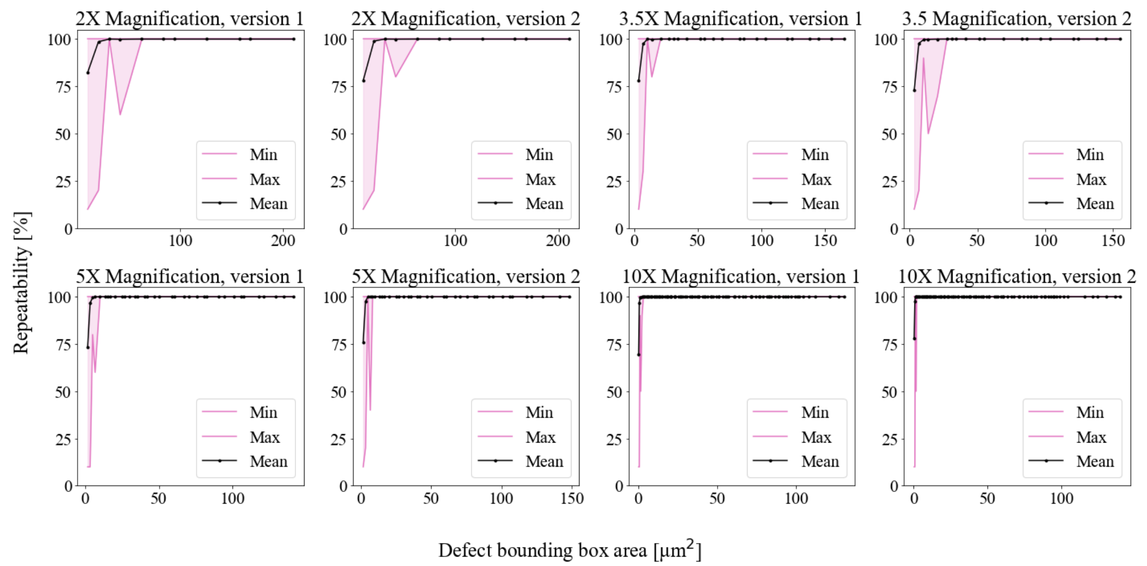

Figure 22. The relative smallest defect bounding box areas which are detected with a 90 % probability in array care area.

By comparing Figures 21 and 22, a difference between logic and array care areas could be seen. Logic care area was more sensitive to variation in repeatability whereas array care area had less variation in repeatability. Relative defect bounding box areas where the average repeatability was at least 90 % are tabulated for each care area, magnification, and recipe version in Table 6. The result of 5X magnification with recipe version 1 characteristics in logic care area was used as a reference to which other defect bounding box areas were scaled to. There was a minor effect on the recipe version to the results.

Table 6. The relative smallest defect bounding box areas which are detected with a 90 % probability. The results are tabulated for each care area, magnification, and recipe version. Smallest defect bounding box area in which the repeatability was at least 90 % detected with 5X magnification with recipe version 1 characteristics in logic care area was used as reference to which other defect bounding box areas were scaled to.

Care area	Recipe version	Magnification			
		2X	**3.5X**	**5X**	**10X**
Logic	1	8.33	2.40	1.00	0.29
	2	7.29	2.40	1.17	0.34
Array	1	8.33	2.74	1.33	0.34
	2	8.33	2.74	1.33	0.34

Conclusions about the relative defect bounding box areas with 90 % repeatability could be made with the results in Table 6. Even though logic care area had more variation

than array care area, the minimum defect bounding box areas were smaller. Logic care area might have originally had smaller programmed defects than array care area due to which the minimum defect bounding box areas are smaller and the variation is higher. The changes between recipe versions in terms of minimum defect bounding box areas are minor. They could be explained by the variance between inspections.

The variation of repeatability indicated that other defect attributes could also have an effect to the detection. Therefore, exploratory data analysis was conducted for the repeated inspections of the defect wafers to see the effect of other defect attributes to the repeatability. Figure 23 shows the relationships between the defect attributes and repeatability for the defect wafers provided by Murata Electronics Oy.

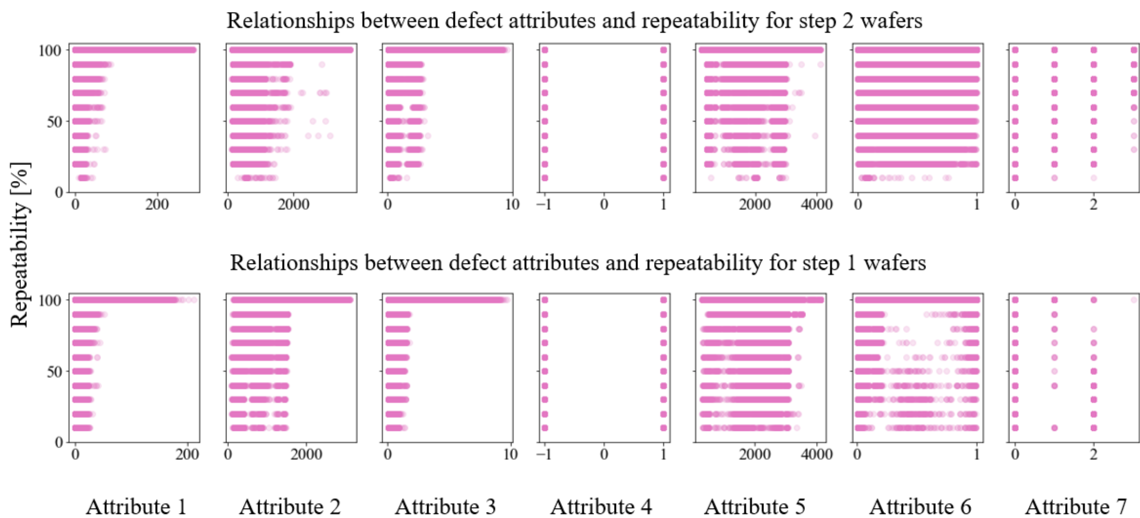

Figure 23. Relationships between defect attributes and repeatability. The upper plots contain merged data from the inspection results of step 2 wafers. The plots below contain merged data from the inspection results of step 1 wafers. Attributes 1, 2, and 3 have similar relationship to repeatability as the defect bounding box area had. The relationship is logarithmic. For attributes 5 and 6, a clear relationship could not be noticed. The relationship to repeatability seems to be random. Attributes 4 and 7 were categorical, and the effect to repeatability seems to be random, also.

Based on the Figure 23 the differences between step 2 and step 1 wafers are minor. It seems that attributes 1, 2, and 3 have the same logarithmic trend as the defect bounding box area had with repeatability. So, the smaller the value for these attributes, the smaller is the probability for a defect to be detected. For attributes 5 and 6, a clear relationship with repeatability cannot be interpreted. The relationship to repeatability appears to be random. Attributes 4 and 7 were categorical, and the effect to the repeatability seems to be random, too.

6.6 Accuracy analysis

Defect attribute accuracy analysis was conducted for the programmed defects in the wafers provided by Murata Electronics Oy. The analysis was done separately for every magnification and recipe version. The results from the repeatability analysis were grouped by defect locations so that relative standard deviation could be calculated separately for each defect. Relative standard deviation defines the ratio between standard deviation and absolute value of the mean. Relative standard deviation enables the comparison between the accuracies of the defect attributes. The relative standard deviation dataframes of step 2 wafers were merged together so that the median relative standard deviation for every defect type could be calculated. Then, the same was repeated for the step 1 wafers. The results of median relative standard deviations for 5X magnification are shown in Tables 7, 8, 9, and 10. The median relative standard deviation results for other magnifications and recipe versions are shown in the Appendix 3.

Table 7. Relative standard deviation medians for the defect attributes. The data contained inspection results for step 2 wafers provided by Murata Electronics Oy. The inspection recipe used 5X magnification and recipe version 1 characteristics.

Defect attribute	Defect type				
	Through crack	Half-through crack	Wider or narrower structure	Missing material	Additional material
1	0.11	0.10	0.22	0.09	0.22
2	0.03	0.04	0.05	0.01	0.03
3	0.05	0.07	0.05	0.02	0.05
5	0.03	0.04	0.02	0.01	0.01
6	0.03	0.04	0.02	0	0.01
X-coordinate	0	0	< 0.01	< 0.01	0.01
Y-coordinate	< 0.01	< 0.01	< 0.01	< 0.01	0.01
Area	0.08	0.11	0.34	0.05	0.34

Table 8. Relative standard deviation medians for the defect attributes. The data contained inspection results for step 2 wafers provided by Murata Electronics Oy. The inspection recipe used 5X magnification and recipe version 2 characteristics.

Defect attribute	Defect type				
	Through crack	Half-through crack	Wider or narrower structure	Missing material	Additional material
1	0.06	0.07	0.11	0.14	0.17
2	0.03	0.04	0.03	0.01	0.03
3	0.04	0.06	0.24	0.03	0.05
5	0.02	0.03	0.03	0.02	0.03
6	0.01	0.04	0.04	< 0.01	< 0.01
X-coordinate	< 0.01	< 0.01	< 0.01	< 0.01	0.01
Y-coordinate	< 0.01	< 0.01	< 0.01	< 0.01	0.01
Area	0.08	0.09	0.14	0.06	0.33

Table 9. Relative standard deviation medians for the defect attributes. The data contained inspection results for step 1 wafers provided by Murata Electronics Oy. The inspection recipe used 5X magnification and recipe version 1 characteristics.

Defect attribute	**Defect type**				
	Through crack	Half-through crack	Wider or narrower structure	Missing material	Additional material
1	0.06	0.06	0.09	0.12	0.23
2	0.01	0.02	0.04	0.03	0.04
3	0.01	0.03	0.17	0.07	0.10
5	0.01	0.02	0.14	0.05	0.07
6	0.02	0.05	0.04	< 0.01	< 0.01
X-coordinate	< 0.01	0	< 0.01	< 0.01	< 0.01
Y-coordinate	< 0.01	< 0.01	< 0.01	< 0.01	< 0.01
Area	0.08	0.11	0.08	0.18	0.33

Table 10. Relative standard deviation medians for the defect attributes. The data contained inspection results for step 1 wafers provided by Murata Electronics Oy. The inspection recipe used 5X magnification and recipe version 2 characteristics.

Defect attribute	**Defect type**				
	Through crack	Half-through crack	Wider or narrower structure	Missing material	Additional material
1	0.04	0.05	0.09	0.09	0.21
2	0.01	0.02	0.04	0.04	0.04
3	0.01	0.02	0.12	0.08	0.10
5	0.01	0.02	0.09	0.11	0.05
6	0.02	0.05	0.04	0.01	< 0.01
X-coordinate	< 0.01	0	< 0.01	< 0.01	0.008
Y-coordinate	< 0.01	< 0.01	< 0.01	< 0.01	0.01
Area	0.08	0.11	0.08	0.08	0.32

Based on the Tables above (7, 8, 9, 10) and the tables in the Appendix 3, the order from highest relative standard deviation to smallest relative standard deviation is most probably:

1. Defect bounding box area
2. Attribute 1
3. Attribute 3
4. Attribute 5
5. Attribute 2
6. Attribute 6

7. Defect coordinates.

The magnitude of the relative standard deviation appears to be dependent on the magnification and recipe version. The higher the magnification, the smaller were the median relative standard deviations. Respectively, with recipe version 2 characteristics, the median relative standard deviations were smaller.

6.7 Difference image analysis

Difference image shows the difference between reference and test image. The reference image is an image of a healthy MEMS structure, and the test image is an image of the same structure but in different location. So, the test image can have defects. Ideally, the difference between reference and test image would be zero, but in reality, there is always small variation due to changing imaging conditions, for example. In case of a defective test image as in Figure 24, the difference image highlights the defect seen in the test image. Due to the order of subtraction, additional material defects should appear as black in the difference image. On the contrary, missing material defects should appear as white. But as seen in the Figure 24, the additional material defect highlighted in the difference image is not completely black, because the cavity in the reference image and the additional material in the test image have similar pixel values.

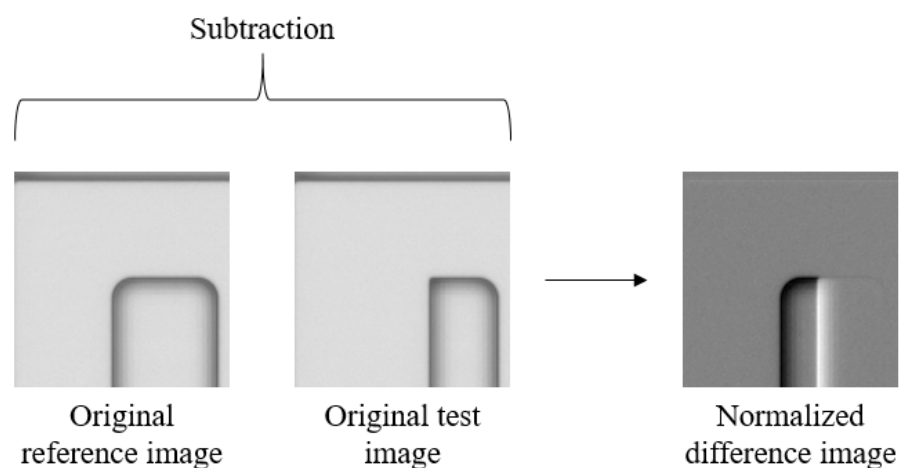

Figure 24. The process in the difference image analysis. Test image is first subtracted from the reference image. The resulting difference image is normalized. Then, the matched difference images are aligned and compared to each other with SSIM.

The difference images were calculated by subtracting the test image from the reference image with Python's cv2 library functions. The resulting difference image was normalized. The difference images retrieved with different wavelengths were matched and aligned to the difference images retrieved with blue light. The alignment was applied by calculating the translation matrix between the images by phase_cross_correlation function. With the translation matrix, the offset could be applied to the pixel matrix by discrete Fourier transform (fft.fftn() function in numpy library) and inverse discrete Fourier transform (fft.ifftn() function in numpy library). Finally, the difference images were cropped such that the final figures contained 70 % of the original difference image. With this the distortion in the edges of the aligned difference images could be removed.

The matched, aligned, and cropped difference images were compared to each other to see, if the difference images were similar to each other. The similarity of two images was measured with Structural Similarity Index (SSIM) which models the structural changes between two images [31]. SSIM can be expressed with the following equation

$$SSIM(x,y) = \frac{(2\mu_x\mu_y + c_1)(2\sigma_{xy} + c_2)}{(\mu_x^2 + \mu_y^2 + c_1)(\sigma_x^2 + \sigma_y^2 + c_2)}, \quad (7)$$

where x and y are the locations in the images, μ_x and μ_y are the averages of x and y, σ_x and σ_y are the variances of x and y, and c_1 and c_2 are variables which stabilize the division [31]. SSIM can range from -1 to 1 where 1 indicates that the compared images are perfectly similar. In Python, SSIM can be calculated with structural_similarity function from skimage.metrics library. The boxplots in Figure 25 show the distribution of SSIM between difference images for each wavelength comparison. Respectively, Figure 26 shows the difference images which had the minimum, median and maximum structural similarity indexes.

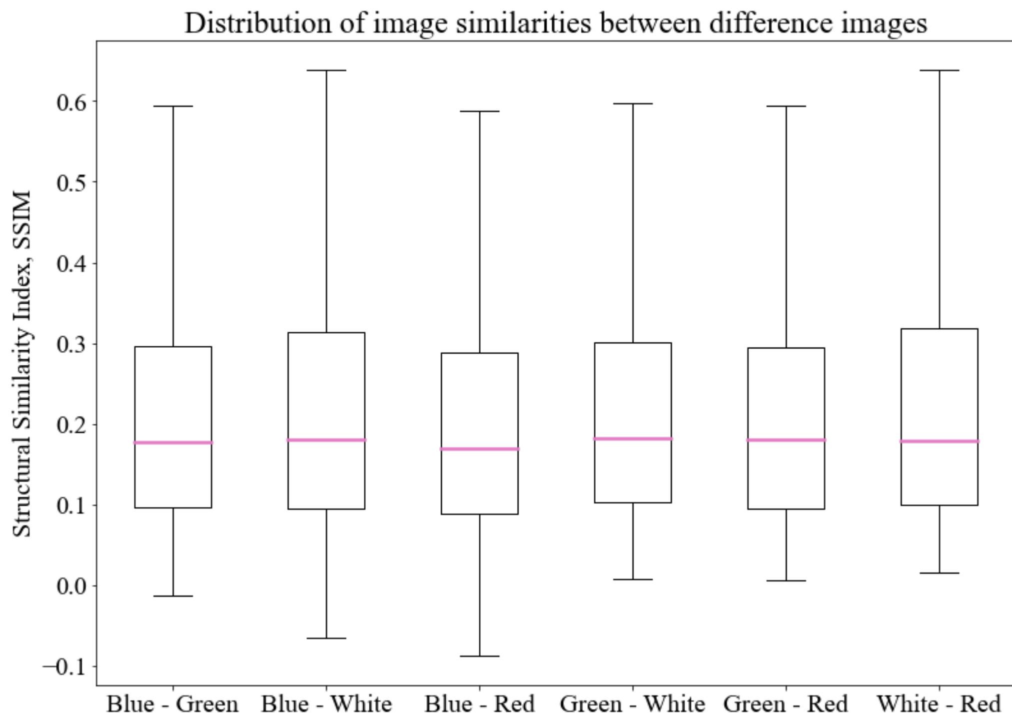

Figure 25. A boxplot showing the similarities between difference images retrieved with different wavelengths. The similarity is measured with SSIM. SSIM can range from -1 to 1 where 1 indicates a perfect similarity.

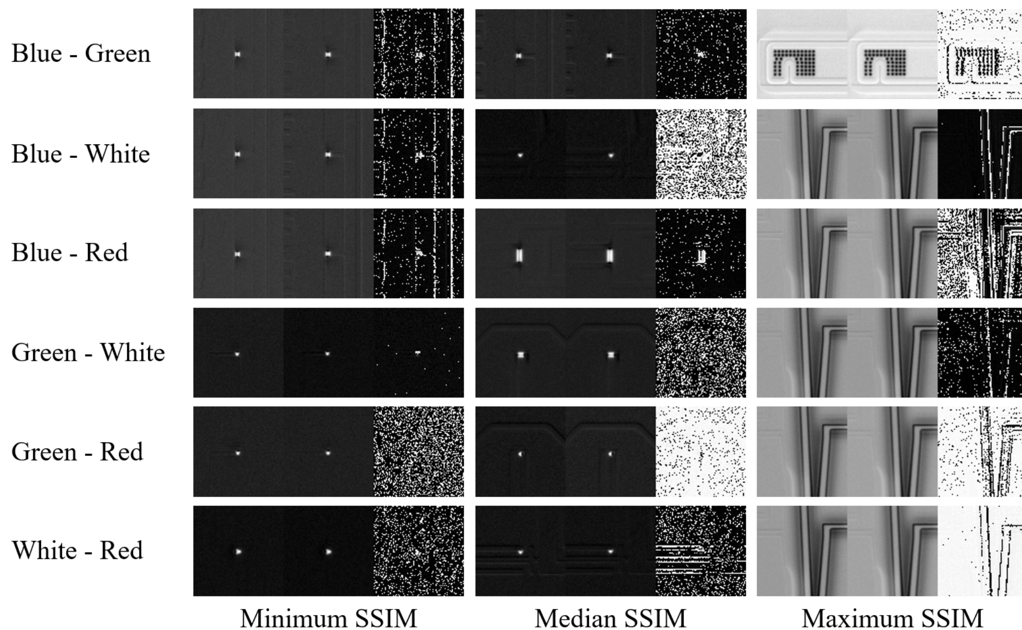

Figure 26. Difference images having the minimum, median, and maximum SSIM values. The first and second small images are the difference images calculated from the reference and test images acquired with a certain wavelengths. The third image is the difference between the first and second images. So in a sense, the third image presents visually the SSIM.

Based on the boxplot in Figure 25, the similarities between difference images range approximately from 0 to 0.7. In other words, the difference images can be thought to be 50-85 % similar. The dissimilarities can arise from the changing imaging conditions and wavelength, for example. The variability between the boxplots is similar. The median SSIM values appear to be approximately at the same level, so the median similarities between different difference image comparisons do not probably differ from each other. Thus, it can be thought that there is not much difference between the similarities in the difference images. However, the smallest SSIM median is achieved when red difference images are compared to the blue difference images. This may be due to the fact that the wavelength difference between red and blue light is the largest. So, perhaps the contrast of the image is worse at one of the two wavelengths. The minimum and median SSIM values were seen with small missing material defects as can be seen in the Figure 26. Highest SSIM values were seen with large missing material defects. Overall, it seems that the wavelength does not have that much of an effect in difference images as the similarities between difference images retrieved with different wavelengths vary almost equally.

7 DISCUSSION

7.1 Current study

The resolution and repeatability analysis of the defect wafer inspection results revealed that the relationship between defect bounding box area and repeatability is logarithmic. The probability for a defect to be detected in repeated inspections is smaller with small defect bounding box areas. Also, the smaller the defect bounding box area, the more there is variation in repeatability. Exploratory data analysis between other defect attributes and repeatability revealed that attributes 1-3 had also logarithmic relationship. For attributes 4-7, the relationship appeared to be random.

The resolution of the equipment is dependent on the magnification and inspection recipe characteristics. The higher the magnification the smaller the resolution. High magnification has small working distance, field of view, and pixel size which allow the detection of smaller defects. Moreover, the probability of detecting small defects has less deviation with higher magnifications. In general, the more sensitive the inspection recipe characteristics the better the resolution. So, with blue light and small thresholds small resolution can be achieved. However, there were some anomalies in the results which impair this observation.

The surface materials of the wafers impact on what is the most optimal choice in terms of the inspection wavelength. For the wafers which had silicon as surface material, blue light resulted in the smallest resolution. However, the uncertainty of resolution was higher with blue light than with white light. For the wafers which had silicon and silicon dioxide as wafer surface materials, the effect in deviation was similar. Though, the smallest resolution was obtained with white light. The surface materials of the defect wafer provided by the AOI equipment manufacturer were silicon and chromium. For this wafer, the difference between blue and white light was not that understandable as the results of the achieved smallest resolutions were anomalous. For 2X and 3.5X magnifications, the smallest resolutions were obtained with blue light and smaller thresholds. For 5X and 10X magnifications, the smallest resolutions were achieved with white light and bigger thresholds.

The anomalies in the reported resolution with the equipment manufacturer defect wafer can be caused by the wafer surface materials. Perhaps, the contrast of the defect images and the SNR between the defect and the background is better with white light even though

the wavelength of white light is longer than the wavelength of blue light. The difference is only observed at 5X and 10X magnifications because the overall deviation in resolution is smaller. Similar anomaly could be seen on the resolution results of the step 2 wafers provided by Murata Electronics Oy. First, it seemed that the resolution is better with recipe version 2 characteristics as 2X and 3.5X magnification had the smallest resolution with this recipe version. However, it was the opposite for 5X and 10X magnifications. So, actually recipe version 1 characteristics obtained the best resolution for the step 2 wafers.

Another anomaly noticed with the defect wafers provided by Murata Electronics Oy was that the resolutions obtained with 10X magnification were bigger than the resolutions obtained with 5X magnification even though it should be the opposite. The reason for this behaviour arises from the thresholds assigned for the 10X magnification inspection recipes. They were almost two times higher compared to the thresholds in 5X magnification recipes.

Small resolution and throughput go hand in hand as small resolution typically increases the inspection time. Therefore the cons of having a sensitive recipe must be discussed. First of all, the defect count is high with sensitive recipe characteristics and big magnification. There is a possibility that DOI's can drown among nuisance defects. In addition, the yield can decrease if the detection of nuisance defects cannot be reduced as healthy elements are falsely classified defective. Secondly, the inspection is slow. For comparison, the inspection of the defect wafers provided by Murata Electronics Oy took half time longer with 10X magnification as with 3.5X or 5X magnification and 5 times longer as with 2X magnification. So, inspecting the whole wafer with 10X magnification and sensitive recipe characteristics impairs the throughput. Therefore, using 10X magnification and sensitive recipe characteristics is worth only for a specific small element area.

The accuracy of the AOI equipment depends on the magnification and recipe characteristics used. The higher the magnification, the smaller the relative standard deviations of the defect attributes. In addition, smaller relative standard deviations can be achieved with more sensitive recipe characteristics. The smallest deviation was obtained for the defect coordinates. The relative standard deviations were mostly below 0.01. The defect bounding box area had the highest uncertainty. This can partly explain the variability in the repeatability figures. It is important to know the relative standard deviations of the defect attributes because it has an effect on the defect classification during inspection postprocessing. If the attributes with high relative standard deviations are used at the beginning of the classification, the classification of the defect can vary much. Instead, if the defect attributes with small relative standard deviations are used at the beginning of the classifi-

cation, the classification has less uncertainty. In other words, false classification of defects can be reduced. Overall, it can be said that the AOI equipment is accurate.

Difference image analysis revealed that the there are only minor differences between images retrieved with different wavelengths. The difference images were 50-85 % similar. The dissimilarities can arise from the changing imaging conditions and wavelength, for example. The biggest difference was detected between blue and red difference images which is reasonable because they have the largest difference in wavelength. The images retrieved with red light have probably better contrast as mentioned in Chapter 3. Based on the results, it cannot be assumed that any of the wavelengths used is clearly inferior in terms of the defect image quality.

7.2 Future work

For the future, similar study could be conducted for capping wafers. Capping wafers are bonded to structure wafers so that the delicate moving structures are protected from particles, and a vacuum can be created. The surface of the capping wafer contains silicon, glass, and different metals due to which the repeatability, resolution, and accuracy results can be different compared to the investigated structure wafers.

The inspection recipe development for the new versions of current products and for the new products in the future, would benefit also from the analysis. By creating a defect wafer, and running the new recipe multiple times, the capability and performance of the new recipe could be evaluated. New products have requirements in terms which is the smallest defect size that should be detected. This should be taken into account while designing the defect wafer. This way, it could be verified that the resolution of the inspection is on the required level.

The research regarding the difference images could be continued. The difference images serve as a good starting point for the construction of a defect classification algorithm. Currently, the inspection recipes export only test images. So, the inspection recipes in the future should export both reference and test images. Then, a large amount of difference images taken from different defects should be manually labeled by defect types. The labeled dataset could be used as a training data for the defect classification algorithm.

8 CONCLUSION

The objectives of the thesis were to determine the capability of the AOI equipment at Murata Electronics Oy in terms of resolution, repeatability, and accuracy. To determine the capability, silicon wafers containing intentionally processed programmed defects were inspected repeatedly. The inspections were conducted for different magnifications and recipe versions so that the full capability of the equipment could be evaluated.

The resolution of the equipment is determined by the light source wavelength, magnification, and recipe characteristics. In general, small resolution is achieved by using short wavelength, big magnification, and sensitive recipe characteristics. However, topography and the material of the defects and the surface of the wafer affect on what is the most optimal wavelength. Therefore, the shortest wavelength may not be the most optimal in terms of resolution. The smallest relative resolution obtained for the equipment manufacturer defect wafer was 0.29. It was achieved with 10X magnification and less sensitive recipe characteristics. For the defect wafers provided by Murata Electronics Oy, the smallest relative resolutions obtained were 0.50 ± 0.00 and 0.56 ± 0.11 for step 2 and step 1 wafers. The resolutions were achieved with 5X magnification. Step 2 wafers had less sensitive recipe characteristics. Step 1 wafers had sensitive recipe characteristics. Resolutions do not have units, because they were scaled to the results obtained with 5X magnification.

The accuracy of the equipment is dependent on the magnification and recipe characteristics used. The higher the magnification, the more accurate the inspection. Sensitive recipe characteristics result in more accurate inspection, too. Defect coordinates had the smallest relative standard deviation whereas defect bounding box area had the highest uncertainty. Difference image analysis revealed that there are only minor difference between defect images retrieved with different wavelengths. However, there is an indication that defect images obtained with red light have the best contrast.

Overall, the capability of the equipment can be improved by dividing the inspection into multiple tests. For the element areas which require the detection of small defects, 10X magnification, short wavelength, and sensitive recipe characteristics can be used. For other element areas, lower magnification, longer wavelength, and less sensitive recipe characteristics are sufficient. The optimal inspection light for wafers having silicon as surface material was blue light. For the wafers with silicon and chromium or silicon and silicon dioxide, the optimal inspection light was white light. After all, the resolution limit regarding visible light can be exceeded with ultraviolet light, x-ray light, or with different inspection techniques such as an automated SEM.

REFERENCES

[1] Rong Sheng Lu, Yan Qiong Shi, Qi Li, and Qing Ping Yu. Aoi techniques for surface defect inspection. *Applied Mechanics and Materials*, 36:297–302, 2010.

[2] H. T. Young, H. S. Chiou, and W. R. Huang. Aoi strategies for defects identification of micro-electro mechanical system elements. *Advances in Materials and Processing Technologies*, 2(2):220–226, 2016.

[3] Xiaoyu Yang, Fuye Dong, Feng Liang, and Guohe Zhang. Chip defect detection based on deep learning method. *2021 IEEE International Conference on Power Electronics, Computer Applications (ICPECA)*, pages 215–219, 2021.

[4] Yang Yuan-Fu. A deep learning model for identification of defect patterns in semiconductor wafer map. *2019 30th Annual SEMI Advanced Semiconductor Manufacturing Conference (ASMC)*, pages 1–6, 2019.

[5] Ralf Buengener. Defect inspection strategies for 14 nm semiconductor technology. *Proc. SPIE 8466, Instrumentation, Metrology, and Standards for Nanomanufacturing, Optics, and Semiconductors VI*, 846607, 2012.

[6] T. Strapacova, R. Priewald, T. Jerman, and C. Mentin. Inline wafer edge inspection system for yield enhancement of thin wafers. *2017 28th Annual SEMI Advanced Semiconductor Manufacturing Conference (ASMC)*, pages 138–143, 2017.

[7] Stephen Lloyd and Martin Lim. The age of sensors - how mems sensors will enable the next wave of new products. *2016 IEEE Symposium on VLSI Technology*, pages 1–4, 2016.

[8] R. Gogue. Mems sensors: past, present and future. *Sensor Review*, 27(1):7–13, 2007.

[9] Jianxiong Zhu, Xinmiao Liu, Qiongfeng Shi, Tianyiyi He, Zhongda Sun, Xinge Guo, Weixin Liu, Othman Bin Sulaiman, Bowei Dong, and Chengkuo Lee. Development trends and perspectives of future sensors and mems/nems. *Micromachines*, 11(1), 2020.

[10] Johannes Richter, Detlef Streitferdt, and Elena Rozova. On the development of intelligent optical inspections. *2017 IEEE 7th Annual Computing and Communication Workshop and Conference (CCWC)*, pages 1–6, 2017.

[11] Douglas B Murphy. *Fundamentals of light microscopy and electronic imaging*. John Wiley & Sons, 2002.

[12] D. W. Piston. Choosing objective lenses: The importance of numerical aperture and magnification in digital optical microscopy. *The Biological Bulletin*, 195(1):1–4, 1998.

[13] Michael W Davidson and Mortimer Abramowitz. Optical microscopy. *Encyclopedia of imaging science and technology*, 2(120):1106–1141, 2002.

[14] Zhonghe Ren, Fengzhou Fang, Ning Yan, and You Wu. State of the art in defect detection based on machine vision. *International Journal of Precision Engineering and Manufacturing-Green Technology*, pages 1–31, 2021.

[15] Franz Pernkopf and Paul O'Leary. Image acquisition techniques for automatic visual inspection of metallic surfaces. *NDT E International*, 36:609–617, 12 2003.

[16] Ziyin Li and Qi Yang. System design for pcb defects detection based on aoi technology. *2011 4th International Congress on Image and Signal Processing*, 4:1988–1991, 2011.

[17] Ralph Neubecker and Jenny E. Hon. Automatic inspection for surface imperfections: requirements, potentials and limits. *Proc. SPIE 10009, Third European Seminar on Precision Optics Manufacturing*, 1000907, 2016.

[18] Vedang Chauhan, Heshan Fernando, and Brian Surgenor. Effect of illumination techniques on machine vision inspection for automated assembly machines. *Proceedings of The Canadian Society for Mechanical Engineering (CSME) International Congress 2014*, pages 1–6, 2014.

[19] Abd Al Rahman M. Abu Ebayyeh and Alireza Mousavi. A review and analysis of automatic optical inspection and quality monitoring methods in electronics industry. *IEEE Access*, 8:183192–183271, 2020.

[20] Ralf Buengener, Julie L. Lee, Brian M. Trapp, and John A. Rudy. A quality metric for defect inspection recipes. *IEEE Transactions on Semiconductor Manufacturing*, 26(1):3–10, 2013.

[21] S. Mir, L. Rufer, and A. Dhayni. Built-in-self-test techniques for mems. *Microelectronics Journal*, 37(12):1591–1597, 2006.

[22] Lee Hong-Ji, Hung Che-Lun, Leng Chia-Hao, Lian Nan-Tzu, Young Ling-Wu, Yang Tahone, Chen Kuang-Chao, and Lee Chih Yuan. Etch defect characterization and reduction in hard-mask-based al interconnect etching. *International Journal of Plasma Science and Engineering*, 2008, 09 2008.

[23] Vikas Chaudhary, Ishan R. Dave, and Kishor P. Upla. Automatic visual inspection of printed circuit board for defect detection and classification. *2017 International Conference on Wireless Communications, Signal Processing and Networking (WiSPNET)*, pages 732–737, 2017.

[24] Beant Kaur, Gurmeet Kaur, and Amandeep Kaur. Detection and classification of printed circuit board defects using image subtraction method. *2014 Recent Advances in Engineering and Computational Sciences (RAECS)*, pages 1–5, 2014.

[25] Anil Katiyar, Sunny Behal, and Japinder Singh. Automated defect detection in physical components using machine learning. *2021 8th International Conference on Computing for Sustainable Global Development (INDIACom)*, pages 527–532, 2021.

[26] Xiaoqing Zheng, Song Zheng, Yaguang Kong, and Jie Chen. Recent advances in surface defect inspection of industrial products using deep learning techniques. *The International Journal of Advanced Manufacturing Technology*, 113(1):35–58, 2021.

[27] Dubravko Miljković. Brief review of self-organizing maps. *2017 40th International Convention on Information and Communication Technology, Electronics and Microelectronics (MIPRO)*, pages 1061–1066, 2017.

[28] D. H. Rao and Patavardhan Prashant Panduranga. A survey on image enhancement techniques: Classical spatial filter, neural network, cellular neural network, and fuzzy filter. *2006 IEEE International Conference on Industrial Technology*, pages 2821–2826, 2006.

[29] Junlong Zhu, Jiamin Liu, Tianlai Xu, Shuai Yuan, Zexu Zhang, Hao Jiang, Honggang Gu, Renjie Zhou, and Shiyuan Liu. Optical wafer defect inspection at the 10 nm technology node and beyond. *International Journal of Extreme Manufacturing*, 4, 2022.

[30] Ndubuisi G Orji, Mustafa Badaroglu, Bryan M Barnes, Carlos Beitia, Benjamin D Bunday, Umberto Celano, Regis J Kline, Mark Neisser, Yaw Obeng, and AE Vladar. Metrology for the next generation of semiconductor devices. *Nature electronics*, 1(10):532–547, 2018.

[31] Zhou Wang, A.C. Bovik, H.R. Sheikh, and E.P. Simoncelli. Image quality assessment: from error visibility to structural similarity. *IEEE Transactions on Image Processing*, 13(4):600–612, 2004.

Appendix 1. Wafer map figures

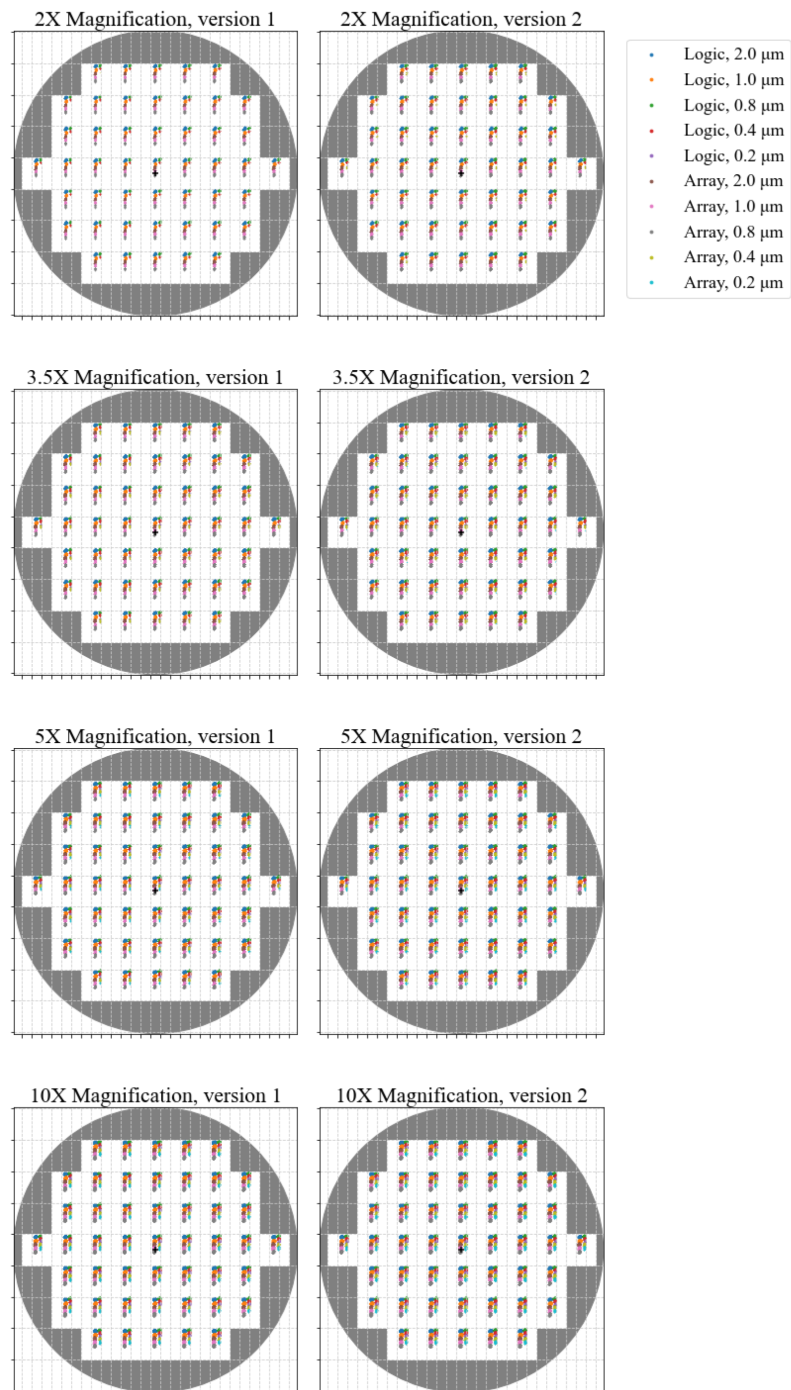

Figure A1.1. Stacked wafer maps of repeated inspections of each magnification and recipe version of the defect wafer provided by the equipment manufacturer. The wafer maps show only the programmed defects.

Appendix 1. (continued)

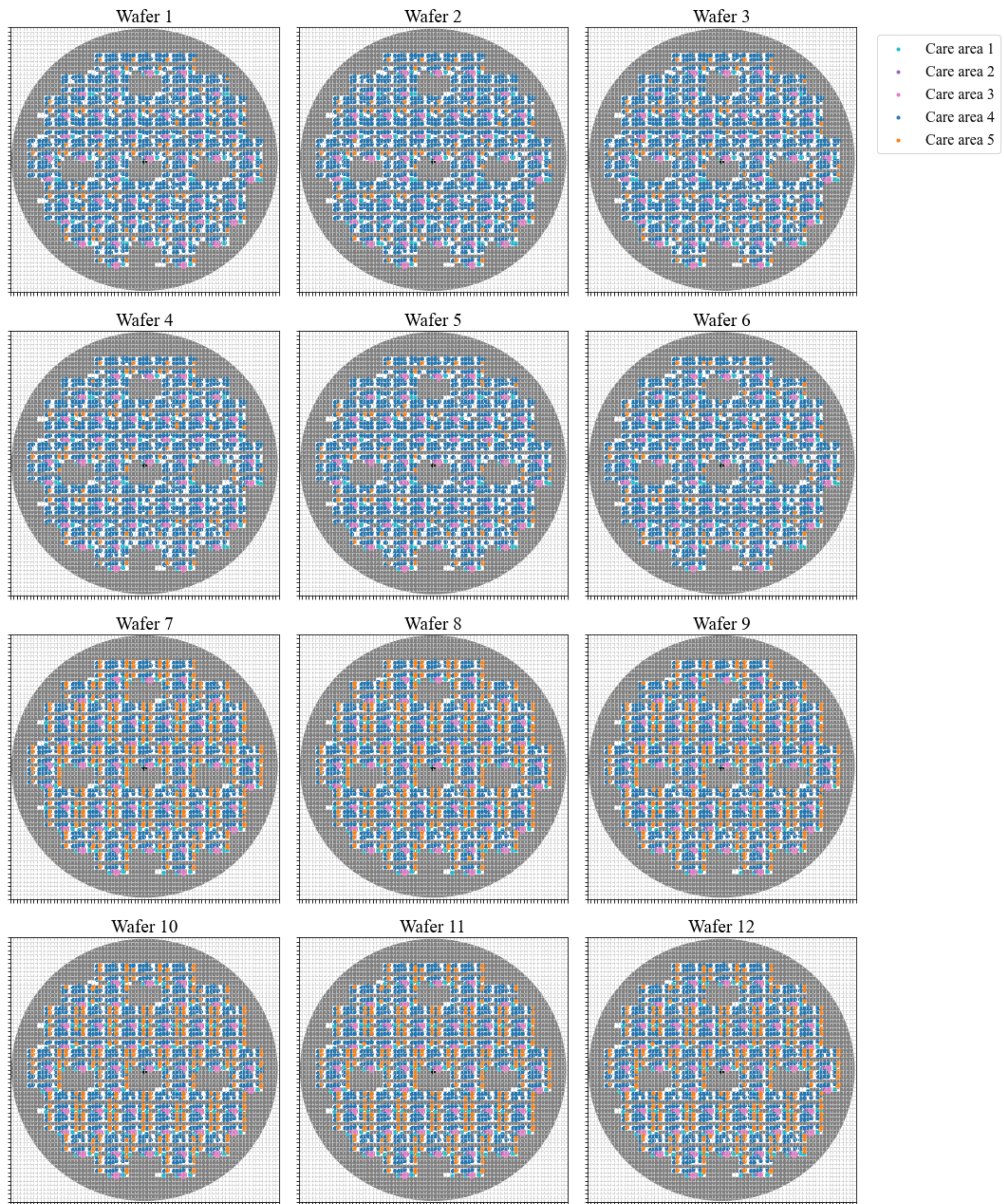

Figure A1.2. Stacked wafer maps of repeated inspections with 2X magnification and recipe version 1 of Murata Electronics Oy defect wafers.

Appendix 1. (continued)

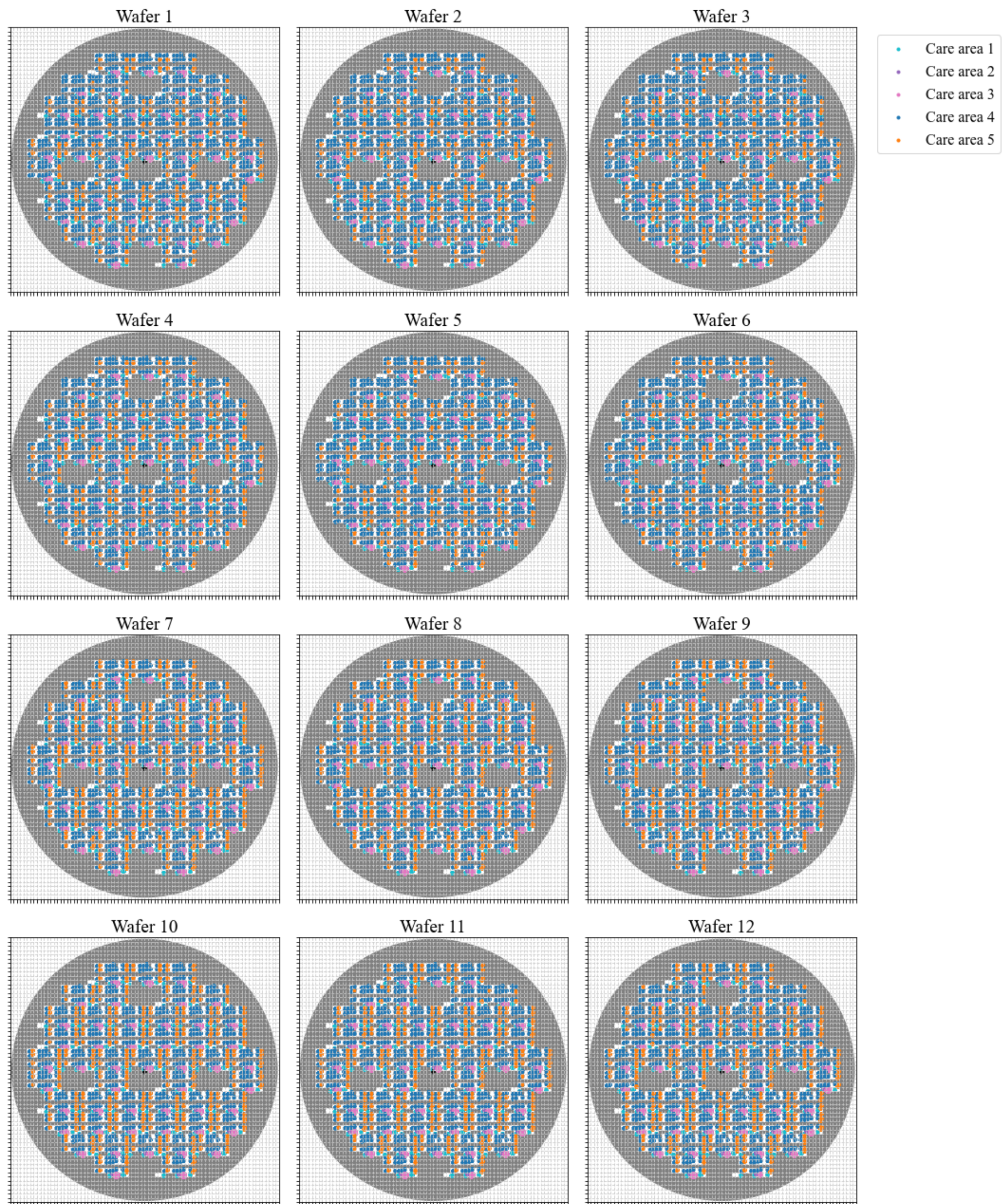

Figure A1.3. Stacked wafer maps of repeated inspections with 2X magnification and recipe version 2 of Murata Electronics Oy defect wafers.

Appendix 1. (continued)

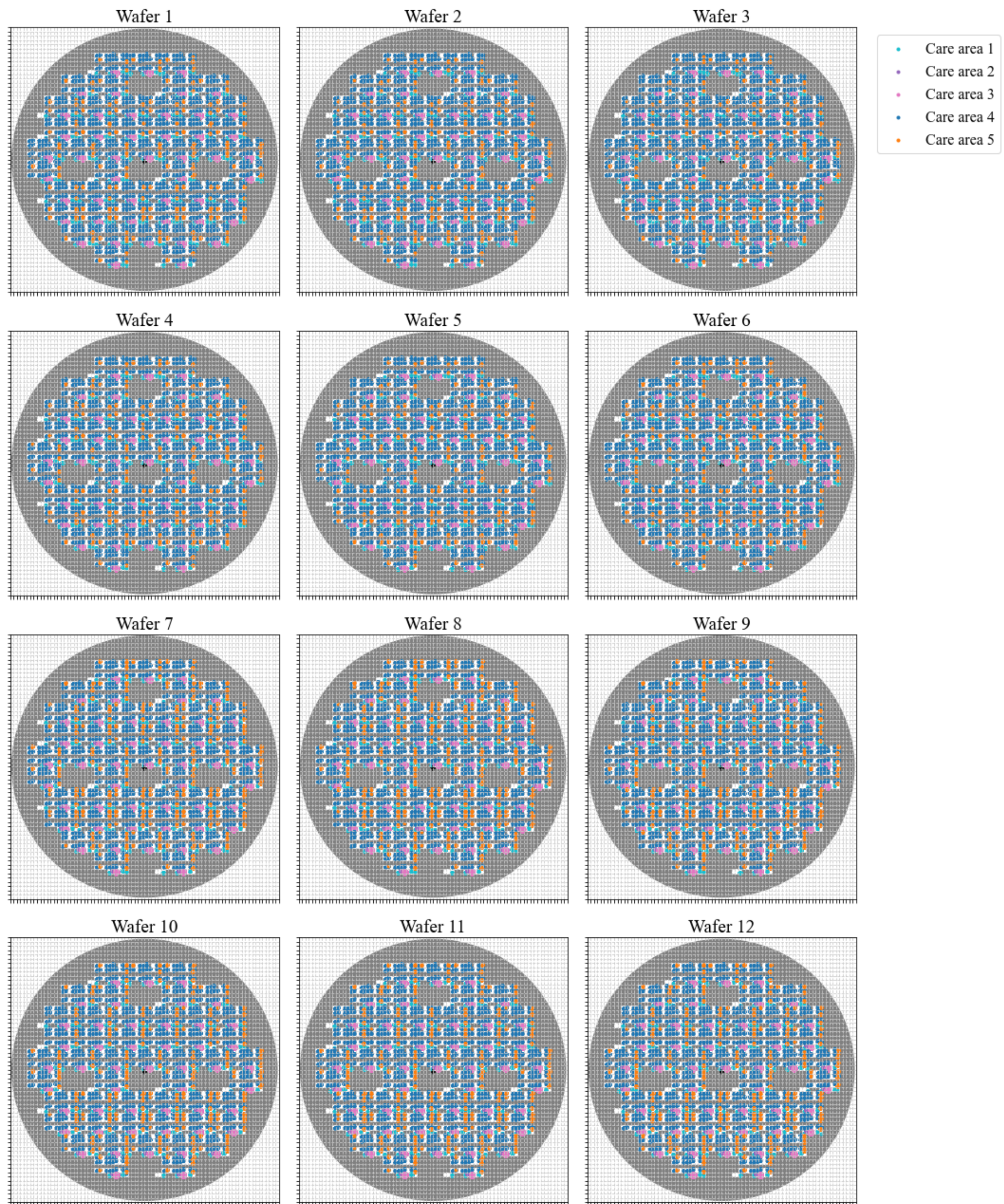

Figure A1.4. Stacked wafer maps of repeated inspections with 3.5X magnification and recipe version 1 of Murata Electronics Oy defect wafers.

Appendix 1. (continued)

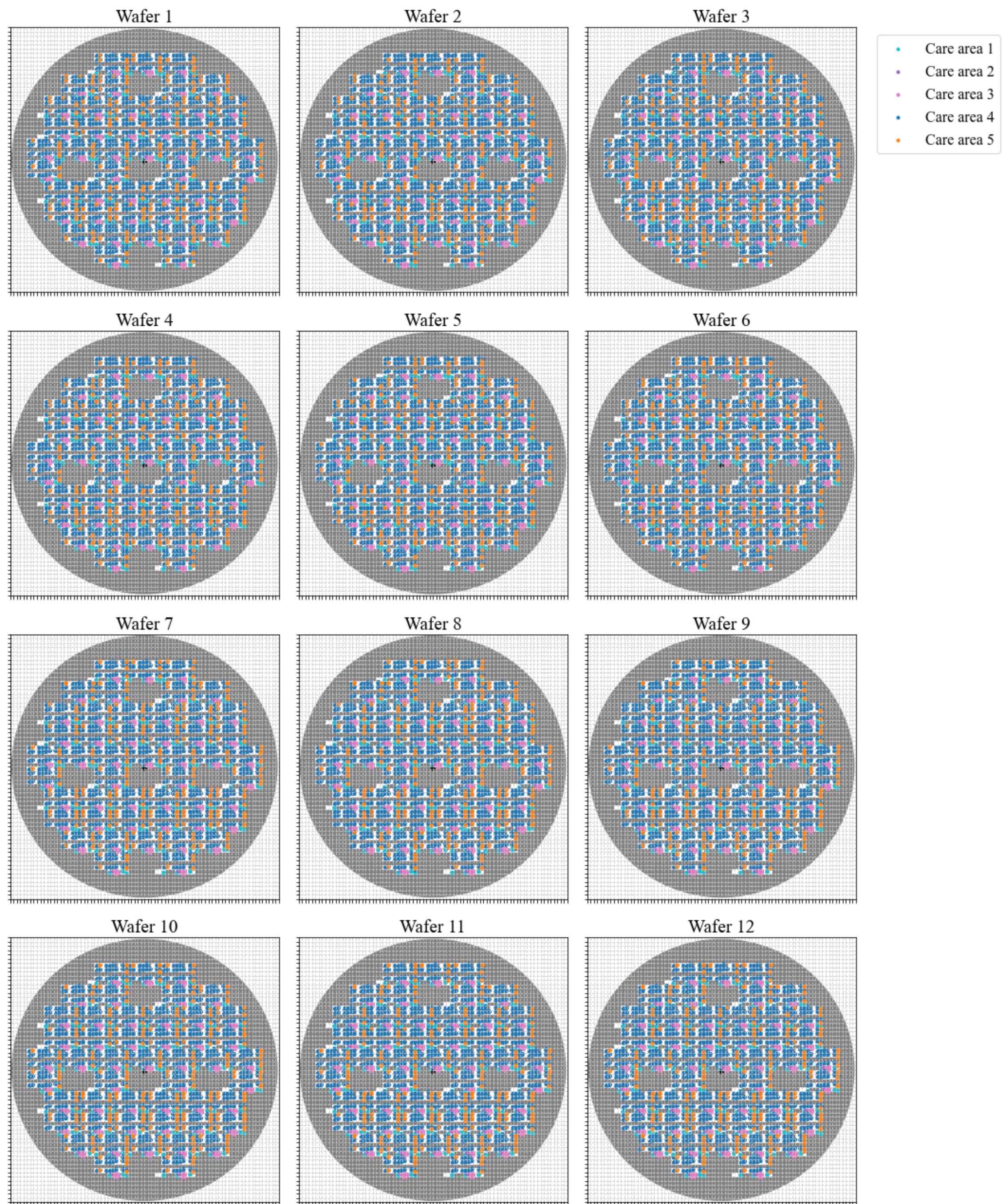

Figure A1.5. Stacked wafer maps of repeated inspections with 3.5X magnification and recipe version 2 of Murata Electronics Oy defect wafers.

Appendix 1. (continued)

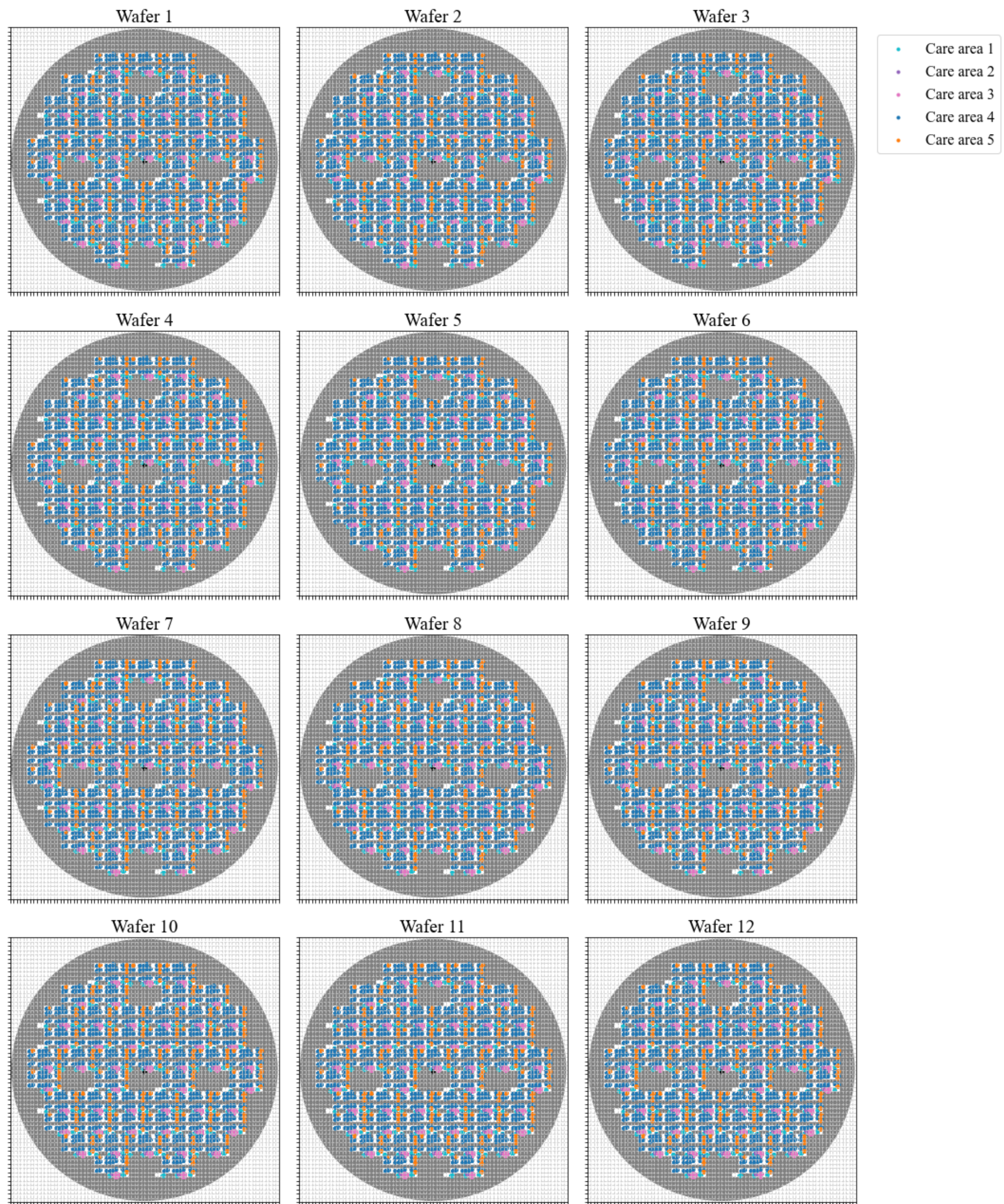

Figure A1.6. Stacked wafer maps of repeated inspections with 5X magnification and recipe version 1 of Murata Electronics Oy defect wafers.

Appendix 1. (continued)

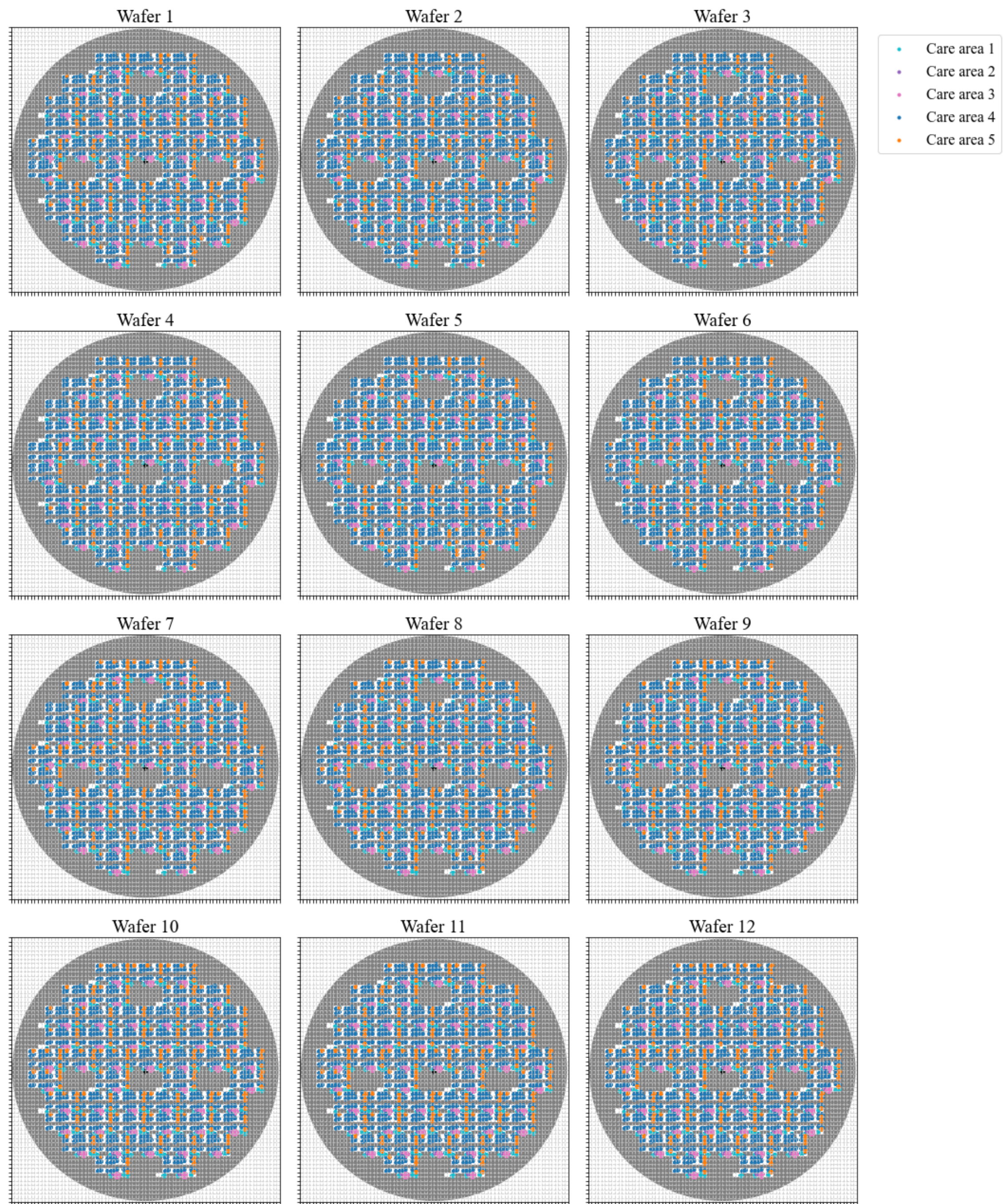

Figure A1.7. Stacked wafer maps of repeated inspections with 5X magnification and recipe version 2 of Murata Electronics Oy defect wafers.

Appendix 1. (continued)

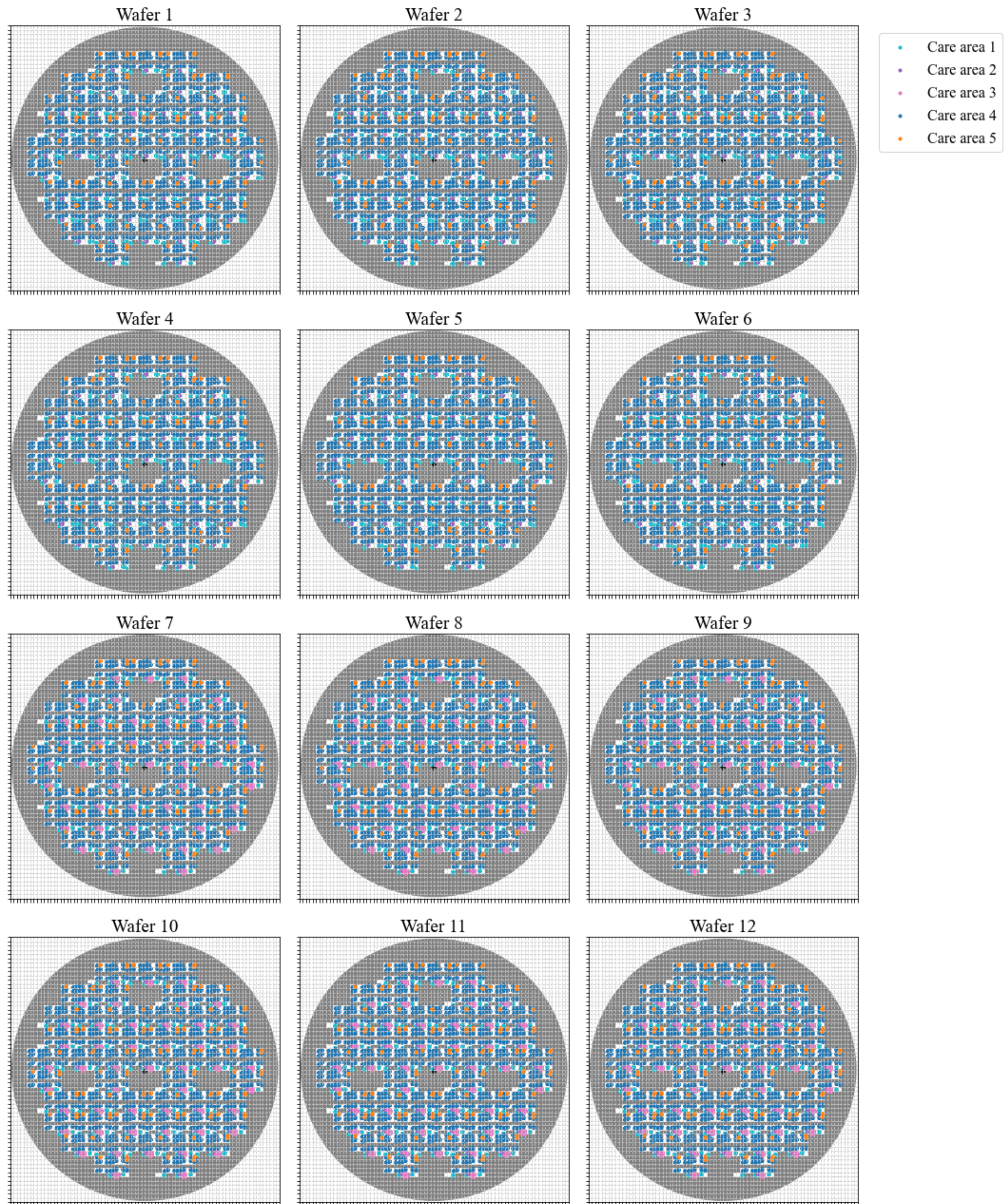

Figure A1.8. Stacked wafer maps of repeated inspections with 10X magnification and recipe version 1 of Murata Electronics Oy defect wafers.

Appendix 1. (continued)

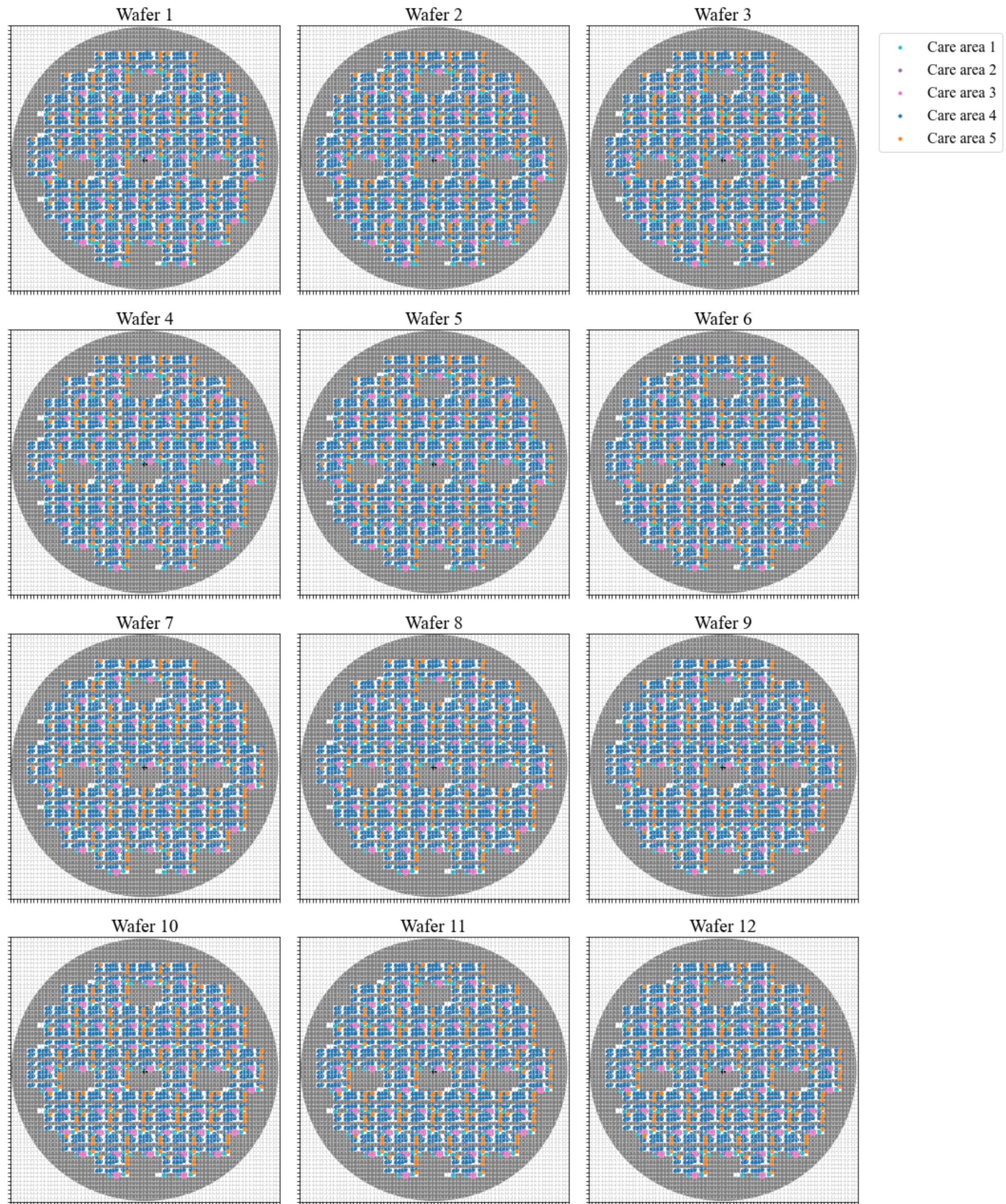

Figure A1.9. Stacked wafer maps of repeated inspections with 10X magnification and recipe version 2 of Murata Electronics Oy defect wafers.

Appendix 2. Stacked die figures

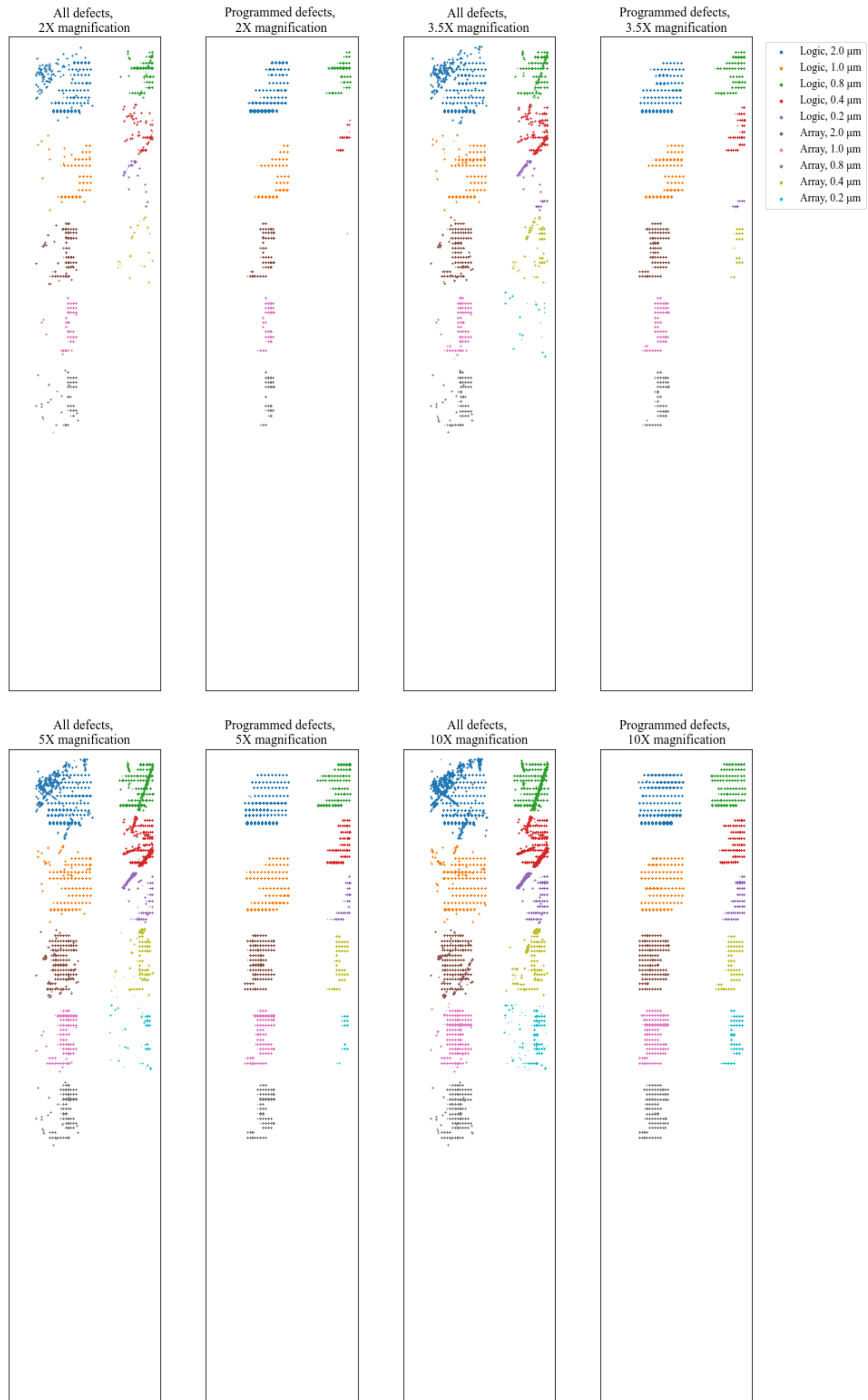

Figure A2.1. Stacked dies of the repeated inspections with recipe version 1 characteristics of the defect wafer provided by the equipment manufacturer.

Appendix 2. (continued)

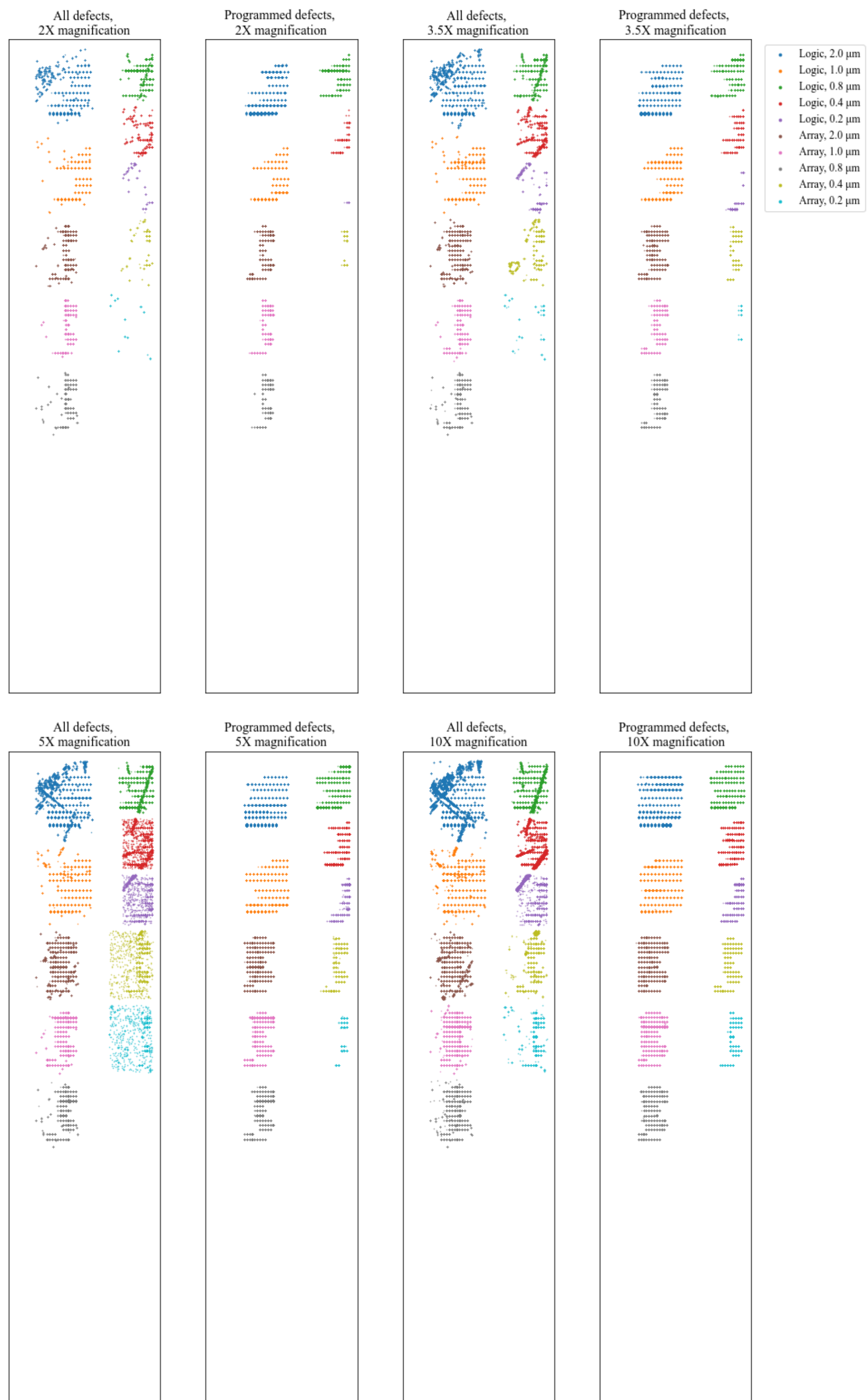

Figure A2.2. Stacked dies of the repeated inspections with recipe version 2 characteristics of the defect wafer provided by the equipment manufacturer.

Appendix 2. (continued)

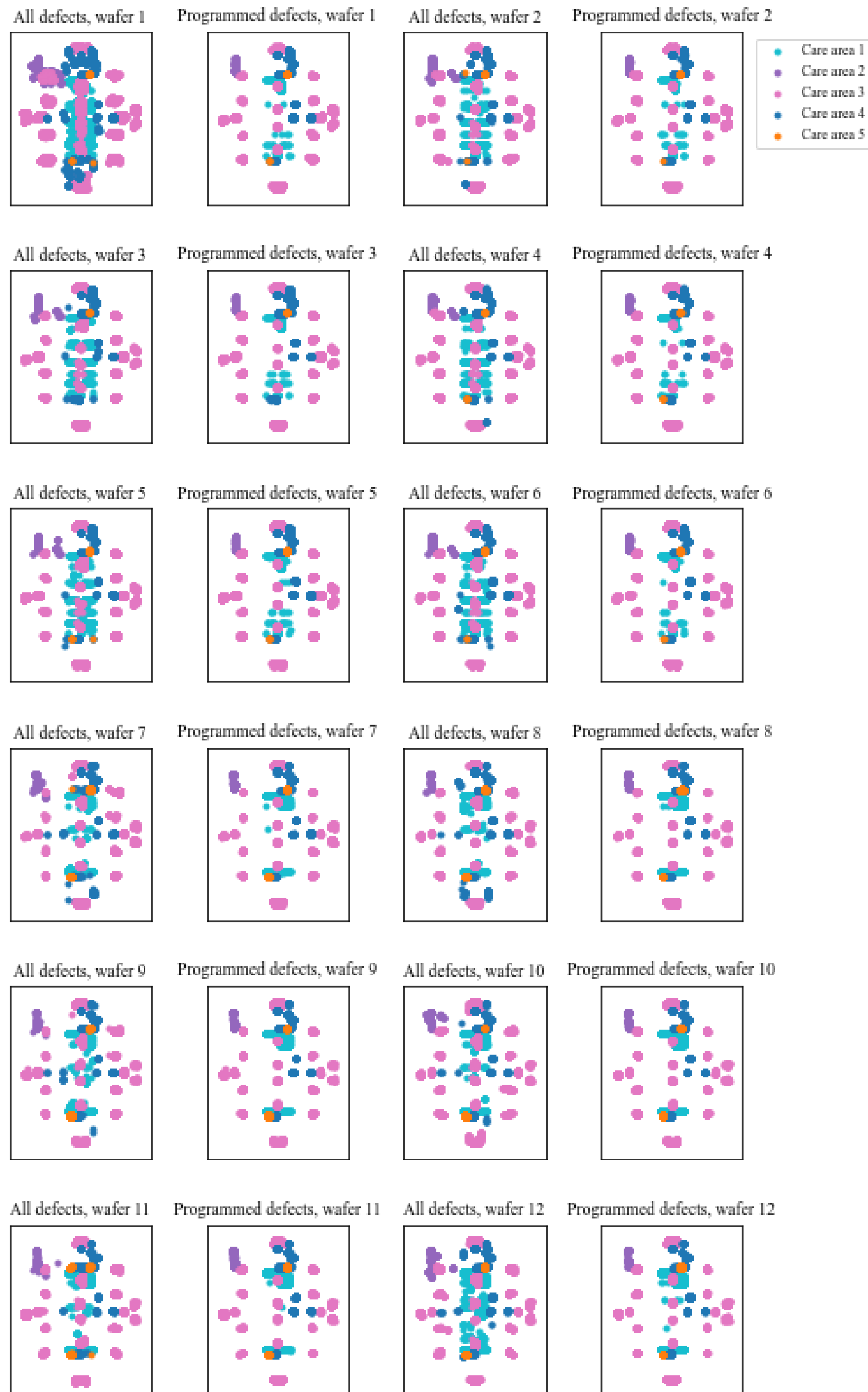

Figure A2.3. Stacked dies of the defect wafers provided by Murata Electronics Oy. The data used in the plotting is from repeated inspections with 2X magnification, recipe version 1. There are two stacked die figures of each wafer - the first stacked die figure shows all defects seen on the wafer and the second stacked die figure shows approximately only the detected programmed defects.

Appendix 2. (continued)

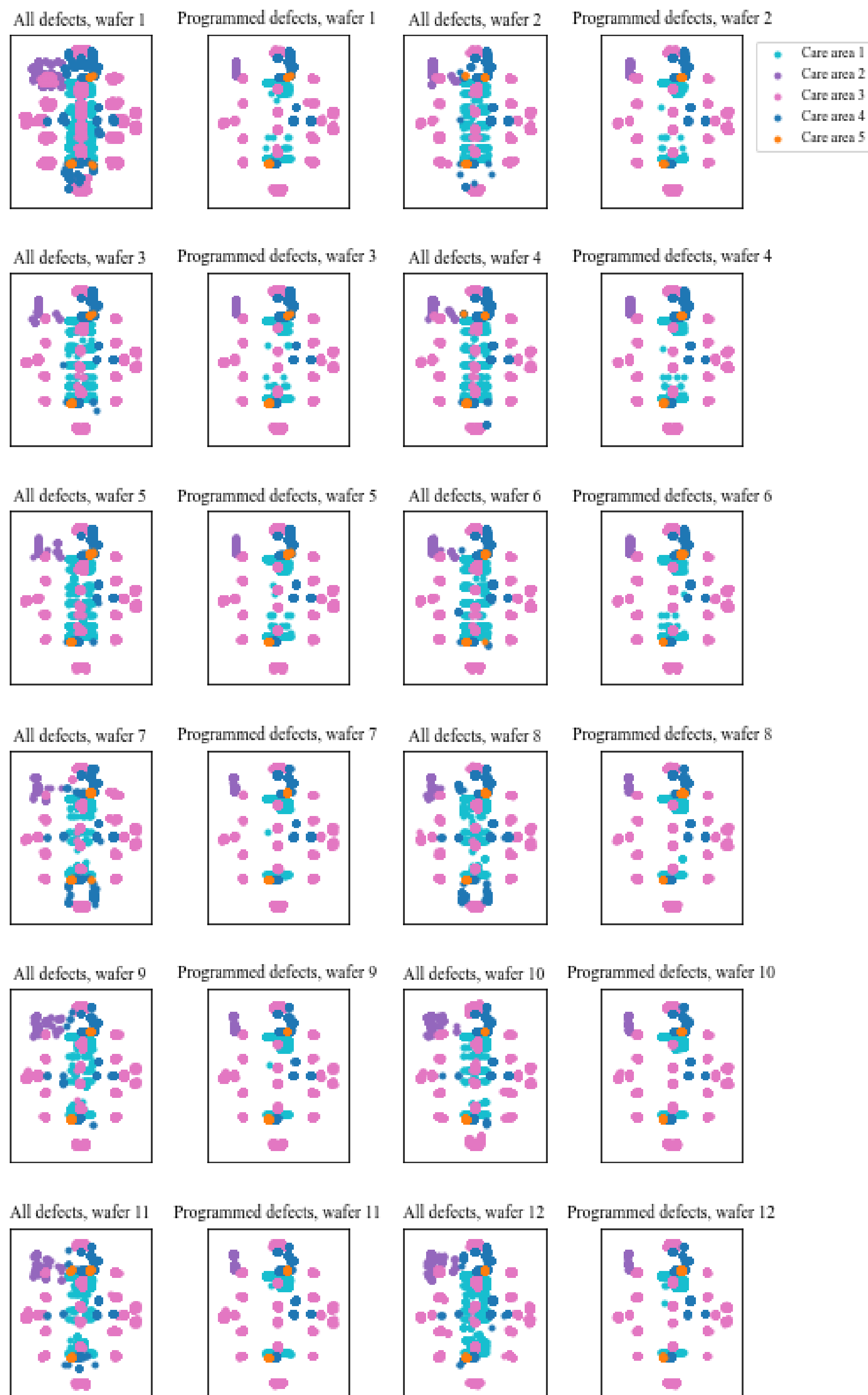

Figure A2.4. Stacked dies of the defect wafers provided by Murata Electronics Oy. The data used in the plotting is from repeated inspections with 2X magnification, recipe version 2. There are two stacked die figures of each wafer - the first stacked die figure shows all defects seen on the wafer and the second stacked die figure shows approximately only the detected programmed defects.

Appendix 2. (continued)

Figure A2.5. Stacked dies of the defect wafers provided by Murata Electronics Oy. The data used in the plotting is from repeated inspections with 3.5X magnification, recipe version 1. There are two stacked die figures of each wafer - the first stacked die figure shows all defects seen on the wafer and the second stacked die figure shows approximately only the detected programmed defects.

Appendix 2. (continued)

Figure A2.6. Stacked dies of the defect wafers provided by Murata Electronics Oy. The data used in the plotting is from repeated inspections with 3.5X magnification, recipe version 2. There are two stacked die figures of each wafer - the first stacked die figure shows all defects seen on the wafer and the second stacked die figure shows approximately only the detected programmed defects.

Figure A2.7. Stacked dies of the defect wafers provided by Murata Electronics Oy. The data used in the plotting is from repeated inspections with 5X magnification, recipe version 1. There are two stacked die figures of each wafer - the first stacked die figure shows all defects seen on the wafer and the second stacked die figure shows approximately only the detected programmed defects.

Appendix 2. (continued)

Figure A2.8. Stacked dies of the defect wafers provided by Murata Electronics Oy. The data used in the plotting is from repeated inspections with 5X magnification, recipe version 2. There are two stacked die figures of each wafer - the first stacked die figure shows all defects seen on the wafer and the second stacked die figure shows approximately only the detected programmed defects.

Appendix 2. (continued)

Figure A2.9. Stacked dies of the defect wafers provided by Murata Electronics Oy. The data used in the plotting is from repeated inspections with 10X magnification, recipe version 1. There are two stacked die figures of each wafer - the first stacked die figure shows all defects seen on the wafer and the second stacked die figure shows approximately only the detected programmed defects.

Appendix 2. (continued)

Figure A2.10. Stacked dies of the defect wafers provided by Murata Electronics Oy. The data used in the plotting is from repeated inspections with 10X magnification, recipe version 2. There are two stacked die figures of each wafer - the first stacked die figure shows all defects seen on the wafer and the second stacked die figure shows approximately only the detected programmed defects.

Appendix 3. Median relative standard deviations for the defect attributes

Table A3.1. Standard deviation medians for the defect attributes. The data used in the standard deviation calculations were merged from datasets 9, 17, 25, 33, 41, and 49. So, the data contained inspection results for step 2 wafers provided by Murata Electronics Oy. The inspection recipe used was 2X magnification with recipe version 1 characteristics.

Defect attribute	**Defect type**				
	Through crack	Half-through crack	Wider or narrower structure	Missing material	Additional material
1	0.12	0.11	0.08	0.19	0.58
2	0.05	0.08	0.07	0.01	0.05
3	0.06	0.09	0.08	0.02	0.10
5	0.01	0.03	0.03	0.02	0.02
6	0.10	0.15	0	0.01	0.23
X-coordinate	< 0.01	< 0.01	< 0.01	< 0.01	0.01
Y-coordinate	< 0.01	< 0.01	< 0.01	< 0.01	0.01
Area	0.21	0.29	0	0.06	0.97

Table A3.2. Standard deviation medians for the defect attributes. The data used in the standard deviation calculations were merged from datasets 57, 65, 73, 81, 89, and 97. So, the data contained inspection results for step 1 wafers provided by Murata Electronics Oy. The inspection recipe used was 2X magnification with recipe version 1 characteristics.

Defect attribute	**Defect type**				
	Through crack	Half-through crack	Wider or narrower structure	Missing material	Additional material
1	0.06	0.06	0.09	0.12	0.23
2	0.01	0.02	0.04	0.03	0.04
3	0.01	0.03	0.17	0.07	0.10
5	0.01	0.02	0.14	0.05	0.07
6	0.02	0.05	0.04	< 0.01	< 0.01
X-coordinate	< 0.01	0	< 0.01	< 0.01	0.01
Y-coordinate	< 0.01	< 0.01	< 0.01	< 0.01	0.01
Area	0.08	0.11	0.08	0.18	0.33

Table A3.3. Standard deviation medians for the defect attributes. The data used in the standard deviation calculations were merged from datasets 10, 18, 26, 34, 42, and 50. So, the data contained inspection results for step 2 wafers provided by Murata Electronics Oy. The inspection recipe used was 2X magnification with recipe version 2 characteristics.

Defect attribute	**Defect type**				
	Through crack	Half-through crack	Wider or narrower structure	Missing material	Additional material
1	0.16	0.18	0.31	0.16	0.26
2	0.06	0.10	0.08	0.02	0.06
3	0.05	0.12	0.11	0.04	0.12
5	0.02	0.06	0.10	0.03	0.06
6	0.08	0.15	0.09	0.01	0.02
X-coordinate	< 0.01	< 0.01	< 0.01	< 0.01	0.01
Y-coordinate	< 0.01	< 0.01	< 0.01	< 0.01	0.01
Area	0.15	0.27	0.46	0.06	0.30

Appendix 3. (continued)

Table A3.4. Standard deviation medians for the defect attributes. The data used in the standard deviation calculations were merged from datasets 58, 66, 74, 82, 90, and 98. So, the data contained inspection results for step 1 wafers provided by Murata Electronics Oy. The inspection recipe used was 2X magnification with recipe version 2 characteristics.

Defect attribute	**Defect type**				
	Through crack	Half-through crack	Wider or narrower structure	Missing material	Additional material
1	0.15	0.17	0.39	0.10	0.27
2	0.05	0.08	0.07	0.01	0.04
3	0.05	0.11	0.19	0.02	0.09
5	0.03	0.07	0.19	0.03	0.05
6	0.04	0.09	0.06	0.01	0.01
X-coordinate	< 0.01	< 0.01	< 0.01	< 0.01	0.01
Y-coordinate	< 0.01	< 0.01	< 0.01	< 0.01	0.01
Area	0.18	0.25	0.18	0.06	0.17

Table A3.5. Standard deviation medians for the defect attributes. The data used in the standard deviation calculations were merged from datasets 11, 19, 27, 35, 43, and 51. So, the data contained inspection results for step 2 wafers provided by Murata Electronics Oy. The inspection recipe used was 3.5X magnification with recipe version 1 characteristics.

Defect attribute	**Defect type**				
	Through crack	Half-through crack	Wider or narrower structure	Missing material	Additional material
1	0.18	0.18	0.18	0.13	0.28
2	0.06	0.08	0.08	0.01	0.02
3	0.10	0.12	0.07	0.03	0.03
5	0.06	0.09	0.03	0.02	0.01
6	0.04	0.10	0.07	0	0.05
X-coordinate	< 0.01	< 0.01	< 0.01	< 0.01	0.01
Y-coordinate	< 0.01	< 0.01	< 0.01	< 0.01	0.01
Area	0.13	0.15	0.45	0.07	0.98

Table A3.6. Standard deviation medians for the defect attributes. The data used in the standard deviation calculations were merged from datasets 59, 67, 75, 83, 91, and 99. So, the data contained inspection results for step 1 wafers provided by Murata Electronics Oy. The inspection recipe used was 3.5X magnification with recipe version 1 characteristics.

Defect attribute	**Defect type**				
	Through crack	Half-through crack	Wider or narrower structure	Missing material	Additional material
1	0.14	0.15	0.15	0.16	0.16
2	0.02	0.05	0.06	0.02	0.03
3	0.02	0.07	0.27	0.03	0.06
5	0.01	0.06	0.27	0.12	0.04
6	0.02	0.07	0.06	0.01	< 0.01
X-coordinate	< 0.01	< 0.01	< 0.01	< 0.01	0.01
Y-coordinate	< 0.01	< 0.01	< 0.01	< 0.01	0.01
Area	0.12	0.17	0.15	0.16	0.32

Appendix 3. (continued)

Table A3.8. Standard deviation medians for the defect attributes. The data used in the standard deviation calculations were merged from datasets 60, 68, 76, 84, 92, and 100. So, the data contained inspection results for step 1 wafers provided by Murata Electronics Oy. The inspection recipe used was 3.5X magnification with recipe version 2 characteristics.

Defect attribute	Defect type				
	Through crack	Half-through crack	Wider or narrower structure	Missing material	Additional material
1	0.10	0.12	0.15	0.17	0.14
2	0.03	0.06	0.07	0.06	0.02
3	0.03	0.07	0.30	0.10	0.05
5	0.01	0.06	0.33	0.09	0.03
6	0.03	0.07	0.06	0.01	< 0.01
X-coordinate	< 0.01	< 0.01	< 0.01	< 0.01	0.01
Y-coordinate	< 0.01	< 0.01	< 0.01	< 0.01	0.01
Area	0.13	0.17	0.14	0.07	0.32

Table A3.7. Standard deviation medians for the defect attributes. The data used in the standard deviation calculations were merged from datasets 12, 20, 28, 36, 44, and 52. So, the data contained inspection results for step 2 wafers provided by Murata Electronics Oy. The inspection recipe used was 3.5X magnification with recipe version 2 characteristics.

Defect attribute	Defect type				
	Through crack	Half-through crack	Wider or narrower structure	Missing material	Additional material
1	0.13	0.16	0.08	0.16	0.15
2	0.06	0.08	0.06	0.02	0.03
3	0.07	0.10	0.20	0.06	0.04
5	0.01	0.04	0.18	0.03	0.02
6	0.03	0.05	0.13	< 0.01	< 0.01
X-coordinate	< 0.01	< 0.01	< 0.01	< 0.01	0.01
Y-coordinate	< 0.01	< 0.01	< 0.01	< 0.01	0.01
Area	0.11	0.15	0.15	0.07	0.32

Table A3.9. Standard deviation medians for the defect attributes. The data used in the standard deviation calculations were merged from datasets 15, 23, 31, 39, 47, and 55. So, the data contained inspection results for step 2 wafers provided by Murata Electronics Oy. The inspection recipe used was 10X magnification with recipe version 1 characteristics.

Defect attribute	Defect type				
	Through crack	Half-through crack	Wider or narrower structure	Missing material	Additional material
1	0.15	0.10	0.26	0.13	0.30
2	0.03	0.03	0.03	0.01	0.04
3	0.07	0.04	0.03	0.02	0.05
5	0.04	0.03	< 0.01	0.02	< 0.01
6	0.03	0.05	0.02	0	0
X-coordinate	< 0.01	< 0.01	< 0.01	< 0.01	< 0.01
Y-coordinate	< 0.01	< 0.01	< 0.01	< 0.01	< 0.01
Area	0.08	0.10	0.13	0.03	0.01

Appendix 3. (continued)

Table A3.10. Standard deviation medians for the defect attributes. The data used in the standard deviation calculations were merged from datasets 63, 71, 79, 87, 95, 103. So, the data contained inspection results for step 1 wafers provided by Murata Electronics Oy. The inspection recipe used was 10X magnification with recipe version 1 characteristics.

Defect attribute	**Defect type**				
	Through crack	Half-through crack	Wider or narrower structure	Missing material	Additional material
1	0.08	0.08	0.10	0.12	0.27
2	0.01	0.01	0.01	0.02	0.08
3	0.01	0.02	0.13	0.04	0.13
5	0.01	0.02	0.09	0.03	0.10
6	0.01	0.11	0.04	< 0.01	< 0.01
X-coordinate	< 0.01	< 0.01	< 0.01	< 0.01	0.01
Y-coordinate	< 0.01	< 0.01	< 0.01	< 0.01	0.01
Area	0.06	0.08	0.18	0.07	0.49

Table A3.11. Standard deviation medians for the defect attributes. The data used in the standard deviation calculations were merged from datasets 16, 24, 32, 40, 48, and 56. So, the data contained inspection results for step 2 wafers provided by Murata Electronics Oy. The inspection recipe used was 10X magnification with recipe version 2 characteristics.

Defect attribute	**Defect type**				
	Through crack	Half-through crack	Wider or narrower structure	Missing material	Additional material
1	0.10	0.07	0.12	0.19	0.50
2	0.03	0.04	0.06	0.01	0.05
3	0.17	0.05	0.06	0.02	0.17
5	0.19	0.03	0.01	0.02	0.04
6	0.03	0.03	0.03	0	0.01
X-coordinate	< 0.01	< 0.01	< 0.01	< 0.01	0.01
Y-coordinate	< 0.01	< 0.01	< 0.01	< 0.01	0.01
Area	0.06	0.08	0.15	0.05	1.21

Table A3.12. Standard deviation medians for the defect attributes. The data used in the standard deviation calculations were merged from datasets 64, 72, 80, 88, 96, and 104. So, the data contained inspection results for step 1 wafers provided by Murata Electronics Oy. The inspection recipe used was 10X magnification with sensitive recipe characteristics.

Defect attribute	**Defect type**				
	Through crack	Half-through crack	Wider or narrower structure	Missing material	Additional material
1	0.07	0.07	0.09	0.09	0.25
2	0.01	0.01	0.01	0.02	0.04
3	0.01	0.02	0.16	0.05	0.09
5	0.01	0.01	0.15	0.03	0.13
6	0.01	0.10	0.05	< 0.01	0.01
X-coordinate	< 0.01	< 0.01	< 0.01	< 0.01	0.01
Y-coordinate	< 0.01	< 0.01	< 0.01	< 0.01	0.01
Area	0.06	0.08	0.36	0.07	0.41